

Precision Matrix Estimation under the Horseshoe-like Prior–Penalty Dual

Ksheera Sagar

Department of Statistics, Purdue University

and

Sayantan Banerjee

Indian Institute of Management, Indore

and

Jyotishka Datta

Department of Statistics, Virginia Polytechnic Institute and State University

and

Anindya Bhadra

Department of Statistics, Purdue University

Abstract

Precision matrix estimation in a multivariate Gaussian model is fundamental to network estimation. Although there exist both Bayesian and frequentist approaches to this, it is difficult to obtain good Bayesian and frequentist properties under the same prior–penalty dual. To bridge this gap, our contribution is a novel prior–penalty dual that closely approximates the graphical horseshoe prior and penalty, and performs well in both Bayesian and frequentist senses. A chief difficulty with the horseshoe prior is a lack of closed form expression of the density function, which we overcome in this article. In terms of theory, we establish posterior convergence rate of the precision matrix that matches the oracle rate, in addition to the frequentist consistency of the MAP estimator. In addition, our results also provide theoretical justifications for previously developed approaches that have been unexplored so far, e.g. for the graphical horseshoe prior. Computationally efficient EM and MCMC algorithms are developed respectively for the penalized likelihood and fully Bayesian estimation problems. In numerical experiments, the horseshoe-based approaches echo their superior theoretical properties by comprehensively outperforming the competing methods. A protein–protein interaction network estimation in B-cell lymphoma is considered to validate the proposed methodology.

Keywords: graphical models; non-convex optimization; posterior concentration; posterior consistency; sparsity.

1 Introduction

High-dimensional precision matrix estimation under a multivariate normal model is a fundamental building block for network estimation, and a common thread connecting disparate applications such as inference on gene regulatory networks (Huynh-Thu and Sanguinetti, 2019), econometrics (Callot et al., 2019; Fan et al., 2016), and neuroscience (Ryali et al., 2012). The frequentist solution to this problem is now relatively well understood and several useful algorithms exist; see Pourahmadi (2011) for a detailed review. However, interested readers will quickly discern that the Bayesian literature on this problem is still sparse, barring some notable exceptions described in Section 1.1. The reason for this is simple: the focus of a Bayesian is on the entire posterior and quantification of uncertainty using the said posterior; a problem fundamentally more demanding computationally. Consequently, the virtues of probabilistic uncertainty quantification notwithstanding, the Bayesian treatment to precision matrix estimation has received relatively scant attention from impatient practitioners. Furthermore, a penalized likelihood estimate with good frequentist properties need not correspond to good Bayesian posterior concentration properties under the corresponding prior. A notable example of this in linear regression models is the lasso penalty (Tibshirani, 1996), and its Bayesian counterpart using the double exponential prior (Park and Casella, 2008), for which Castillo et al. (2015) assert: “the LASSO is essentially non-Bayesian, in the sense that the corresponding full posterior distribution is a useless object.” We address this gap in the literature in the context of graphical models. Our contribution is a novel prior–penalty dual that makes both fully Bayesian and fast penalized likelihood estimation feasible. The key distinguishing feature of our work is that we provide theoretical and empirical support for *both* Bayesian and frequentist solutions to the problem under the same prior–penalty dual. It is shown that the Bayesian posterior as a whole concentrates around the truth and the penalized likelihood point estimate is consistent. To our knowledge, ours is the first work to establish these results using continuous shrinkage priors under an *arbitrary sparsity pattern* in the true precision matrix. This is at a contrast to the current state of the art in theory that imposes additional constraints on the graph, e.g., banded-ness or more general decomposable structures (Banerjee and Ghosal, 2014; Lee and Lee, 2021; Liu and Martin, 2019; Xiang et al., 2015). Typically these assumptions are made for computational and theoretical tractability rather than any intrinsic subject matter knowledge. The reason our work is able to avoid these restrictive assumptions is because we work with continuous “global-local” shrinkage priors and impose sparsity in a weak sense (see, e.g., Bhadra et al., 2019b).

The motivating data set arises from a biological application. Protein–protein interaction networks have been found to play a crucial role in cancer (Ha et al., 2018). One such significant effort in this direction is “The Cancer Genome Atlas” program (Weinstein et al., 2013) that has collected data from over 7,700 patients across 32 different tumor types. From this repository, we retrieve proteomic data of 33 patients with “Lymphoid Neoplasm Diffuse Large B-cell Lymphoma,” which is a cancer that starts in white blood cells and spreads to lymph nodes. Our findings are contrasted with that of Ha et al. (2018).

1.1 The Current State of the Art and Our Contributions in Context

A Gaussian graphical model (GGM) remains popular as a fundamental building block for network estimation because of the ease of interpretation of the resulting precision matrix estimate: an inferred off-diagonal zero corresponds to conditional independence of the two corresponding nodes given the rest (see, e.g., Lauritzen, 1996).

Among the most popular frequentist approaches for estimating GGMs are the graphical lasso (Friedman et al., 2008) and the graphical SCAD (Fan et al., 2009), which are respectively the graphical extensions of the lasso (Tibshirani, 1996) and SCAD (Fan and Li, 2001) penalties in linear models. Similarly, the CLIME estimator of Cai et al. (2011) is a graphical application of the Dantzig penalty (Candès and Tao, 2010). Fan et al. (2016) propose factor-based models for estimation of precision matrices, which are particularly attractive in financial applications where the precision matrix of outcome variables conditioned on some common factors being sparse is a sensible assumption. Alternatively, Callot et al. (2019) opt for a node-wise regression approach using ℓ_1 penalty for minimizing the risk of a Markowitz portfolio. The positive definiteness of their estimate is guaranteed asymptotically, which nevertheless remains hard to establish in finite samples; a common issue with node-wise regression approaches. Zhang and Zou (2014) propose a new empirical loss termed the *D-trace loss* to avoid computing the log determinant term in the ℓ_1 penalized loss. Under certain conditions they also prove that the resulting estimate is identical to the CLIME estimate (Cai et al., 2011). A ridge type estimate for precision matrix termed ROPE is proposed by Kuismin et al. (2017), who use the squared Frobenius norm of the precision matrix as a penalty function. Another distribution free version of the ridge estimate is proposed by Wang et al. (2015). An elastic net penalty (Zou and Hastie, 2005) is used to determine the functional connectivity among brain regions by Ryali et al. (2012). A comprehensive theoretical treatment for the rate of convergence of precision matrix estimates is given by Lam and Fan (2009).

The frequentist approaches listed above generally enjoy faster and more scalable computation,

owing to being point estimates. Nevertheless, from a Bayesian perspective, a common theme with these penalized approaches is that the posterior concentration properties of the corresponding priors remain completely unexplored. Moving now to Bayesian methodologies for *unstructured precision matrices*, the literature is relatively scant. Wang (2012) proposes a Bayesian version of the graphical lasso and uses a clever decomposition of the precision matrix to facilitate block Gibbs sampling and to guarantee the positive definiteness of the resulting estimate. Banerjee and Ghosal (2015) consider a similar prior structure as the Bayesian graphical lasso, with the exception that they put a large point-mass at zero for the off-diagonal elements of the precision matrix. Under assumptions of sparsity, they derive posterior convergence rates in the Frobenius norm, and also provide a Laplace approximation method for computing marginal posterior probabilities of models. Spike-and-slab variants with double exponential priors is proposed by Gan et al. (2019). A common issue with the spike-and-slab approach is the presence of binary indicator variables, which typically hinder posterior exploration and the Bayesian lasso estimate is known to be biased for large signals. Both of these issues are addressed by the graphical horseshoe estimate proposed by Li et al. (2019), which is an application of the popular global-local horseshoe prior (Carvalho et al., 2010) in GGMs. Li et al. (2019) provide considerable empirical evidence of superior performance over several competing Bayesian and frequentist approaches. Nevertheless, their theoretical results are limited to upper bounds on some Kullback–Leibler risk properties and the bias of the resulting estimate. Consequently, whether the graphical horseshoe posterior has correct concentration properties has remained an open question. Similarly, its frequentist dual: the penalized likelihood estimate, also remains unavailable, mainly because there is no closed form of the horseshoe prior or penalty; only a normal scale mixture representation. Both of these issues are resolved in the present paper. We propose a novel prior–penalty dual that closely approximates the graphical horseshoe prior with the density being available explicitly as well as a normal scale mixture, which has important implications in theory and in practice, and in both Bayesian and frequentist settings. Moreover, as a corollary to one of our main results, the posterior concentration properties of the graphical horseshoe is also established, for the first time.

2 Formulation of the Prior–Penalty Dual

We begin the formal treatment by pointing the interested readers to Supplementary Section S.1 for a summary of mathematical notations used in the paper. Let $\mathbf{X}^{(n)} = (\mathbf{X}_1, \dots, \mathbf{X}_n)^T$ be a random sample from a p -dimensional normal distribution with mean $\mathbf{0}$ and a positive definite

covariance matrix Σ . The corresponding precision matrix, or the inverse covariance matrix $\Omega = ((\omega_{ij}))$ is defined as $\Omega = \Sigma^{-1}$. The natural estimator of Σ is $S = n^{-1} \sum_{i=1}^n \mathbf{X}_i \mathbf{X}_i^T$. We assume that Ω is sparse, in the sense that the number of non-zero off-diagonal elements is small. We utilize the duality between a Bayesian prior and penalty, where the penalized likelihood estimate is understood to correspond to the maximum a posteriori (MAP) estimate under a given prior. Hence, for fully Bayesian inference on Ω , we need a suitable prior that also results in a penalty function with good frequentist properties; a non-trivial problem even in linear models (Castillo et al., 2015). We put independent horseshoe-like priors (Bhadra et al., 2019a) on the off-diagonal and non-informative priors on the diagonal elements of Ω , while restricting the prior mass to positive definite matrices. A key benefit of the horseshoe-like prior, which closely mimics the sparsity-inducing global-local horseshoe prior (Carvalho et al., 2010) is that the prior density, and hence the penalty, is available in closed form under the former, unlike under the latter. This allows one to study the penalty (equivalently, the negative logarithm of the prior density) directly, and to establish important properties concerning convexity (see, e.g., Lemma 4.8), which remain much more difficult under the horseshoe prior. For the fully Bayesian model, the element-wise prior specification induced by the horseshoe-like prior is,

$$\omega_{ij} \mid a \sim \pi(\omega_{ij} \mid a), \quad 1 \leq i < j \leq p; \quad \omega_{ii} \propto 1, \quad 1 \leq i \leq p, \quad (1)$$

where $\pi(\omega_{ij}; a) = \log \left(1 + a/\omega_{ij}^2 \right) / (2\pi a^{1/2})$ gives the horseshoe-like density function for ω_{ij} . The motivation for using this density is two-fold: it has a sharp spike near zero, encoding the Bayesian prior belief that most signals are ignorable; and it also possesses very heavy, polynomially decaying tails, allowing for identification of signals. These two properties closely mimic the popular horseshoe prior for sparse signals (Carvalho et al., 2010), and, in fact, one achieves the same origin and tail rates for the density function in terms of ω_{ij} as in the original horseshoe. The crucial advantage with the horseshoe-like, then, is that there is a closed form to the density function, unlike the horseshoe prior. Nevertheless, similar to the original horseshoe prior, the horseshoe-like prior also admits a convenient latent variable representation as a Gaussian scale-mixture (Bhadra et al., 2019a). To be precise, one can write,

$$\omega_{ij} \mid \nu_{ij}, a \sim \mathcal{N} \left(0, \frac{a}{2\nu_{ij}} \right), \quad \pi(\nu_{ij}) = \frac{1 - \exp(-\nu_{ij})}{2\pi^{1/2}\nu_{ij}^{3/2}}, \quad (2)$$

where marginalizing over the latent ν_{ij} leads to the desired $\pi(\omega_{ij}; a)$ identified above. For modeling valid precision matrices, we must restrict the prior mass on the space of symmetric positive

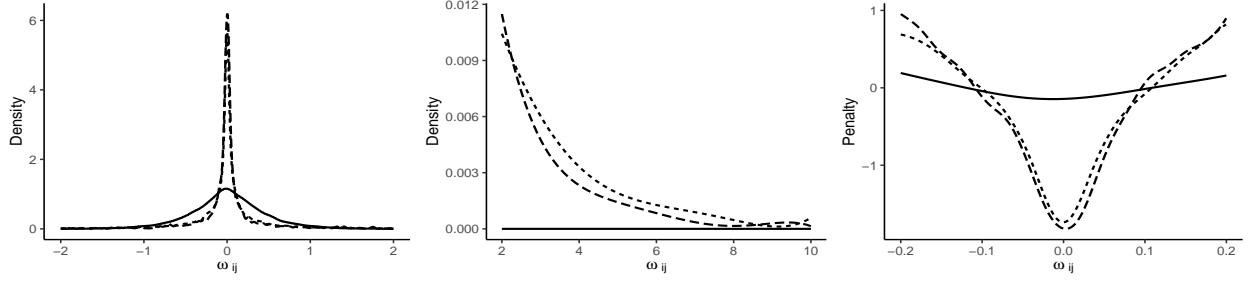


Figure 1: Smoothed density estimates of a randomly chosen off-diagonal element based on 10^4 Markov chain Monte Carlo samples for the graphical horseshoe-like (dashes), the graphical horseshoe (small dashes) and the Bayesian graphical lasso (solid) priors; providing a visual comparison of (left) spikes near the origin, (middle) heaviness of the tails, and (right) the induced penalty functions for $p = 10$.

definite matrices \mathcal{M}_p^+ . Combining the unrestricted prior as in (1) and (2), along with the above restriction, leads to the joint prior specification on Ω as,

$$\pi(\Omega \mid \nu; a)\pi(\nu) \propto \prod_{i,j:i < j} \{1 - \exp(-\nu_{ij})\} \nu_{ij}^{-1} \exp\left(\frac{-\nu_{ij}\omega_{ij}^2}{a}\right) \mathbb{1}_{\mathcal{M}_p^+}(\Omega), \quad (3)$$

where $\nu = \{\nu_{ij}\}_{i < j}$. In this formulation, the latent parameters ν_{ij} are component-specific, or local, and the shared parameter a is global, situating the horseshoe-like in the broader category of global-local priors (Bhadra et al., 2019b). Further details on the induced marginal prior on Ω are presented in Supplementary Section S.2. Although it is possible to put a further hyperprior on a , it is considered fixed for point estimation approaches, and is estimated by the effective model size approach of Piironen and Vehtari (2017) to avoid a collapse to zero. We defer the details to Supplementary Section S.6. With the prior specification as in (3), the log-posterior \mathcal{L} thus becomes,

$$\mathcal{L} \propto \frac{n}{2} \log \det \Omega - \frac{n}{2} \text{tr}(\mathbf{S}\Omega) + \sum_{i,j:i < j} \left\{ \log(1 - \exp(-\nu_{ij})) - \log \nu_{ij} - \frac{\nu_{ij}\omega_{ij}^2}{a} \right\}. \quad (4)$$

At this point, the corresponding hierarchy of the horseshoe prior, which the horseshoe-like closely approximates, is well worth mentioning. The horseshoe prior (Carvalho et al., 2010), recognized as a state-of-the-art for sparse signal recovery (Bhadra et al., 2019a), was deployed in estimating GGMs by Li et al. (2019) with the following hierarchy:

$$\omega_{ij} \mid \lambda_{ij}, \tau \sim \mathcal{N}(0, \lambda_{ij}^2 \tau^2), \quad \pi(\lambda_{ij}^2) \sim \mathcal{C}^+(0, 1), \quad \pi(\tau^2) \sim \mathcal{C}^+(0, 1), \quad (5)$$

where $\mathcal{C}^+(0, 1)$ denotes the standard half-Cauchy distribution. It is recognized as the state of

the art in sparse signal recovery in linear models (Bhadra et al., 2019a), and was successfully deployed in estimating sparse precision matrices by Li et al. (2019). Figure 1 plots the smoothed histogram of prior densities of a randomly chosen off-diagonal element near the origin and at the tails for the graphical horseshoe-like along with two of its relatives: the graphical horseshoe (Li et al., 2019) and the Bayesian graphical lasso (Wang, 2012). The corresponding penalties, given by the negative of the logarithm of the densities, are also shown. The key observations are: (a) the graphical horseshoe and graphical horseshoe-like densities are very similar and (b) both have far sharper spikes near the origin and heavier tails compared to the Laplace priors used in the Bayesian graphical lasso, providing an intuitive basis for the superiority of the horseshoe-family in sparse signal recovery. Extensive formal support for these observations are available in linear models (Bhadra et al., 2019b), but barring some empirical evidence, the corresponding theoretical support is lacking in graphical models.

Some comments on the desirability of a Gaussian scale mixture representation are also in order. First, the latent mixing variables make it easier to derive fully Bayesian computational strategies via data augmentation. A similar observation is true for point estimates via the expectation-maximization algorithm. Second, using a result of Barndorff-Nielsen et al. (1982), it is possible to derive a precise connection between the densities of the mixing variables and that of the resultant mixture. In particular, if the mixing densities are regularly varying in the tails, then so is the resultant Gaussian mixture. Since regular variation is closed under many nonlinear transformations, the heavier tails of global-local priors impart crucial robustness properties for estimating nonlinear, many-to-one functions of the parameters of interest in multi-parameter problems (Bhadra et al., 2016), and help avoid marginalization paradoxes of Dawid et al. (1973).

3 Estimation Procedure

3.1 ECM Algorithm for MAP Estimation

We utilize the Gaussian mixture representation of the horseshoe-like prior with latent scale parameters to devise an Expectation Conditional Maximization (ECM) (Meng and Rubin, 1993) approach to MAP estimation, building on the calculations for linear models by Bhadra et al. (2019a). For updating the elements of the precision matrix, we use the coordinate descent technique proposed by Wang (2014), which guarantees the positive definiteness of the precision matrix at each update.

E Step: Following Bhadra et al. (2019a), we calculate the conditional expectation of the latent

variable ν_{ij} , $1 \leq i < j \leq p$, at current iteration (t) as follows:

$$\nu_{ij}^{(t)} = \mathbb{E}(\nu_{ij} \mid \omega_{ij}^{(t)}, a) = \left(\log \left(1 + \frac{a}{(\omega_{ij}^{(t)})^2} \right) \right)^{-1} \frac{a^2}{\left((\omega_{ij}^{(t)})^2 + a \right) \left((\omega_{ij}^{(t)})^2 \right)}. \quad (6)$$

CM Steps: Having updated the latent parameters in the E-Step, the coordinate descent approach of Wang (2014) is used to update one column of the precision matrix at a time. Without loss of generality, we present the steps for updating the p th column. First we divide the precision matrix $\mathbf{\Omega}$ and the sample covariance matrix \mathbf{S} into blocks as follows:

$$\mathbf{\Omega} = \begin{bmatrix} \mathbf{\Omega}_{11} & \mathbf{\Omega}_{12} \\ \mathbf{\Omega}_{12}^T & \Omega_{22} \end{bmatrix}, \quad n\mathbf{S} = \begin{bmatrix} \mathbf{S}_{11} & \mathbf{S}_{12} \\ \mathbf{S}_{12}^T & S_{22} \end{bmatrix},$$

where, $\mathbf{\Omega}_{11}$ is a matrix of dimension $(p-1) \times (p-1)$ of the top left block of $\mathbf{\Omega}$; Ω_{22} is the p th diagonal element and $\mathbf{\Omega}_{12}$ is a $(p-1) \times 1$ dimensional vector of the remaining elements in the p th column. The decomposition of $n\mathbf{S}$ is analogous. We define $\gamma = \Omega_{22} - \mathbf{\Omega}_{12}^T \mathbf{\Omega}_{11}^{-1} \mathbf{\Omega}_{12}$ and $\boldsymbol{\beta} = \mathbf{\Omega}_{12}$. With these transformations, we simplify (4) to update the p th column. We have,

$$\begin{aligned} \log \det \mathbf{\Omega} &= \log(\gamma) + c_1, \\ \text{tr}(n\mathbf{S}\mathbf{\Omega}) &= 2\mathbf{S}_{12}^T \boldsymbol{\beta} + S_{22}\gamma + S_{22}\boldsymbol{\beta}^T \mathbf{\Omega}_{11}^{-1} \boldsymbol{\beta} + c_2, \\ \sum_{i,j:i < j} \frac{\nu_{ij}^{(t)}}{a} \cdot \omega_{ij}^2 &= \boldsymbol{\beta}^T \mathbf{\Lambda}^{(t)} \boldsymbol{\beta} + c_3, \\ \mathbf{\Lambda}^{(t)} &= \frac{1}{a} \text{diag} \left(\nu_{1p}^{(t)}, \dots, \nu_{p-1,p}^{(t)} \right), \end{aligned} \quad (7)$$

where c_1, c_2, c_3 are constants independent of $\boldsymbol{\beta}, \gamma$. Now the log-posterior with the transformed variables is given by,

$$\mathcal{L} \propto \frac{n}{2} \log(\gamma) - \frac{1}{2} (2\mathbf{S}_{12}^T \boldsymbol{\beta} + S_{22}\gamma + S_{22}\boldsymbol{\beta}^T \mathbf{\Omega}_{11}^{-1} \boldsymbol{\beta}) - \boldsymbol{\beta}^T \mathbf{\Lambda}^{(t)} \boldsymbol{\beta}.$$

Maximizing the above over $\boldsymbol{\beta}, \gamma$ gives the required update as:

$$\hat{\gamma} = \frac{n}{S_{22}}, \quad \hat{\boldsymbol{\beta}} = -(S_{22}\mathbf{\Omega}_{11}^{-1} + 2 \cdot \mathbf{\Lambda}^{(t)})^{-1} \mathbf{S}_{12}^T. \quad (8)$$

Having updated $\boldsymbol{\beta}, \gamma$ from (8), the p th column update of the precision matrix for the next iteration $(t+1)$ becomes

$$\hat{\mathbf{\Omega}}_{12}^{(t+1)} = \hat{\boldsymbol{\beta}}, \quad \hat{\mathbf{\Omega}}_{12}^{T(t+1)} = \hat{\boldsymbol{\beta}}^T, \quad \hat{\Omega}_{22}^{(t+1)} = \hat{\gamma} + \hat{\boldsymbol{\beta}}^T \mathbf{\Omega}_{11}^{-1} \hat{\boldsymbol{\beta}}. \quad (9)$$

We repeat the above steps for the remaining $(p-1)$ columns to complete the CM Step updates for

Algorithm 1 ECM algorithm for MAP estimation (GHS-LIKE-ECM)

```

function ECM FOR GRAPHICAL HORSESHOE-LIKE PENALTY( $\Omega_s, \mathbf{S}, n, p$ )
     $\Omega_s = ((\omega_{s,ij}))$ : starting point;  $\Omega_u = ((\omega_{u,ij}))$ : updated precision matrix; initially set to  $\mathbf{I}_p$ .
     $\mathbf{S} = \mathbf{X}^{(n)T} \mathbf{X}^{(n)} / n$ ;  $\mathbf{N} = ((N_{ij}))$ : A matrix of dimension  $p \times p$  which stores
     $\mathbb{E}(\nu_{ij} \mid \omega_{s,ij}, a)$ ;  $(n, p)$ : Sample size and number of variables respectively
    while  $\Delta = \|\Omega_u - \Omega_s\|_2 < \text{tolerance} (= 10^{-3})$  do
        for  $j = 2 \rightarrow p$  do
            for  $i = 1 \rightarrow (j - 1)$  do
                 $N_{ij} := \mathbb{E}(\nu_{ij} \mid \omega_{s,ij}, a) = \left( \log \left( 1 + \frac{a}{(\omega_{s,ij})^2} \right) \right)^{-1} \frac{(a)^2}{((\omega_{s,ij})^2 + a)((\omega_{s,ij})^2)}.$ 
            end for
        end for
         $\mathbf{N} \leftarrow \mathbf{N} + \mathbf{N}^T$ . This is required to compute  $\Lambda^{(t)}$  in display (7); Set  $\Omega_u = \Omega_s$ 
        for  $i = 1 \leftarrow p$  do
            Update  $i^{th}$  column of  $\Omega_u$  using coordinate descent algorithm of Wang (2014) de-
            scribed above.
        end for
    end while
    return  $\hat{\Omega}^{\text{MAP}} = \Omega_u$ 
end function

```

Ω , until convergence to the MAP estimator $\hat{\Omega}^{\text{MAP}}$. The procedure is summarized in Algorithm 1. The most computationally expensive step is the required inverse of a $(p - 1) \times (p - 1)$ matrix to compute $\hat{\beta}$ in (8), which needs to be repeated for each of the p columns, giving a per iteration complexity of $O(p^4)$ for the algorithm.

3.2 Posterior Sampling for the Fully Bayesian Estimate

For fully Bayesian estimation, we also outline the MCMC sampling procedure. With substitutions $2\nu_{ij} \mapsto t_{ij}^2$ and $a \mapsto \tau^2$, the prior in (2) can be written with a different hierarchy as follows:

$$\omega_{ij} \mid \nu_{ij}, \tau \sim \mathcal{N}(0, \tau^2 / t_{ij}^2), \quad \pi(t_{ij}) = \frac{1 - \exp(-t_{ij}^2/2)}{(2\pi)^{1/2} t_{ij}^2}, \quad t_{ij} \in \mathbb{R}, \quad \tau^2 > 0,$$

where $\pi(t_{ij})$ above is known as the slash normal density, expressed as $(\phi(0) - \phi(t_{ij}))/t_{ij}^2$, where $\phi(\cdot)$ is the standard normal density (Bhadra et al., 2019a). Introducing a further local latent variable r_{ij} , the density for t_{ij} can also be written as a normal scale mixture, where the scale follows a Pareto distribution, that is,

$$t_{ij} \mid r_{ij} \sim \mathcal{N}(0, r_{ij}), \quad r_{ij} \sim \text{Pareto}(1/2).$$

For efficient sampling, the above Pareto scale mixture can be represented as a product of an exponential density and an indicator function as follows:

$$\pi(t_{ij}) = \frac{1}{2} \int_1^\infty \frac{1}{(2\pi r_{ij})^{1/2}} \exp\left(-\frac{t_{ij}^2}{2r_{ij}}\right) r_{ij}^{-3/2} dr_{ij} = \frac{1}{2(2\pi)^{1/2}} \int_0^1 \exp\left(-\frac{t_{ij}^2 m_{ij}}{2}\right) dm_{ij},$$

$$\text{i.e., } \pi(t_{ij}, m_{ij}) = \frac{1}{2(2\pi)^{1/2}} \exp\left(-\frac{t_{ij}^2 m_{ij}}{2}\right) \mathbb{1}(0 < m_{ij} < 1).$$

Different choices of prior for the global scale parameter are possible, but we consider $\tau \sim \mathcal{C}^+(0, 1)$.

[Makalic and Schmidt \(2015\)](#) observed that: if $\tau^2 \mid \xi \sim \text{InvGamma}(1/2, 1/\xi)$ and $\xi \sim \text{InvGamma}(1/2, 1)$ then marginally $\tau \sim \mathcal{C}^+(0, 1)$. Using this, we can write the posterior updates of τ , ξ as follows:

$$\tau^2 \mid \xi, \mathbf{X}^{(n)}, \boldsymbol{\Omega}, \{t_{ij}\}_{i < j}, \{m_{ij}\}_{i < j} \sim \text{InvGamma}((p(p-1)/2 + 1)/2, 1/\xi + \sum_{i,j:i < j} t_{ij}^2 \omega_{ij}^2 / 2),$$

$$\xi \mid \tau \sim \text{InvGamma}(1 + 1/\tau^2).$$
(10)

Following the remaining updates from the graphical horseshoe sampler of [Li et al. \(2019\)](#), the complete MCMC scheme for the graphical horseshoe-like is as outlined in Algorithm 2. The per iteration complexity of the algorithm is $O(p^4)$. Diagnostic plots for both the ECM and MCMC algorithms are given in Supplementary Section S.7.

4 Theoretical Properties

4.1 Posterior Concentration Results

In this section, we present our main result on the posterior contraction rate of the precision matrix $\boldsymbol{\Omega}$ around the true precision matrix $\boldsymbol{\Omega}_0$ with respect to the Frobenius norm under the graphical horseshoe-like prior. The technique of our proofs uses the general theory on posterior convergence rates as outlined in [Ghosal et al. \(2000\)](#), which establishes the desired convergence with respect to the Hellinger distance. However, from the perspective of a precision matrix, the Frobenius norm is easier to interpret in comparison to the Hellinger distance. Under suitable assumptions on the eigenspace of the precision matrices, [Banerjee and Ghosal \(2015\)](#) showed that these two distances are equivalent, and hence the same posterior contraction rates hold with respect to the Frobenius norm as well. We assume that the true underlying graph is sparse, so that the corresponding true precision matrix $\boldsymbol{\Omega}_0$ has s non-zero off-diagonal elements. The total number of non-zero elements in $\boldsymbol{\Omega}_0$ is $p + s$, which gives the effective dimension of the parameter $\boldsymbol{\Omega}_0$. To establish the

Algorithm 2 The Graphical Horseshoe-Like MCMC Sampler (GHS-LIKE-MCMC)

```

function GHS-LIKE( $\mathbf{S}, n, burnin, nmc$ ) ▷ where  $\mathbf{S} = \mathbf{X}^{(n)T} \mathbf{X}^{(n)} / n$ ,  $n$  = sample size
|   Set  $p$  to be number of rows (or columns) in  $\mathbf{S}$ 
|   Set initial values  $\mathbf{\Omega} = \mathbf{I}_p$ ,  $\mathbf{\Sigma} = \mathbf{I}_p$ ,  $\mathbf{T} = \mathbf{1}^T \mathbf{1}$ ,  $\mathbf{M} = \mathbf{1}^T \mathbf{1}$ ,  $\tau = 1$ , where  $\mathbf{1}$  is a  $p$ -dimensional
|   vector with all elements equal to 1,  $\mathbf{T} = ((t_{ij}^2))$ ,  $\mathbf{M} = ((m_{ij}))$ .
|   for  $iter = 1$  to  $(burnin + nmc)$  do
|       for  $i = 1$  to  $p$  do
|            $\gamma \sim \text{Gamma}(\text{shape} = n/2 + 1, \text{rate} = 2/s_{ii})$  ▷ sample  $\gamma$ 
|            $\mathbf{\Omega}_{(-i)(-i)}^{-1} = \mathbf{\Sigma}_{(-i)(-i)} - \boldsymbol{\sigma}_{(-i)i} \boldsymbol{\sigma}'_{(-i)i} / \sigma_{ii}$ 
|            $\mathbf{C} = [s_{ii} \mathbf{\Omega}_{(-i)(-i)}^{-1} + (\text{diag}(\tau^2 / t_{(-i)i}))^{-1}]^{-1}$ 
|            $\boldsymbol{\beta} \sim \text{Normal}(-\mathbf{C} \mathbf{S}_{(-i)i}, \mathbf{C})$  ▷ sample  $\boldsymbol{\beta}$ 
|            $\boldsymbol{\omega}_{(-i)i} = \boldsymbol{\beta}$ ,  $\omega_{ii} = \gamma + \boldsymbol{\beta}^T \mathbf{\Omega}_{(-i)(-i)}^{-1} \boldsymbol{\beta}$  ▷ variable transformation
|            $t_{(-i)i} \sim \text{Gamma}(\text{shape} = 3/2, \text{rate} = m_{(-i)i}/2 + \boldsymbol{\omega}_{(-i)i}^2 / 2\tau^2)$  ▷ sample  $t$ , where  $t_{(-i)i}$ 
|           is a vector of length  $(p-1)$  with entries  $t_{ji}^2, j \neq i$ 
|            $\mathbf{m}_{(-i)i} \sim \text{Exponential}(\text{rate} = t_{(-i)i}/2)$  ▷ sample  $m$ 
|           Save updated  $\mathbf{\Omega}$ 
|            $\mathbf{\Sigma}_{(-i)(-i)} = \mathbf{\Omega}_{(-i)(-i)}^{-1} + (\mathbf{\Omega}_{(-i)(-i)}^{-1} \boldsymbol{\beta})(\mathbf{\Omega}_{(-i)(-i)}^{-1} \boldsymbol{\beta})' / \gamma$ ,  $\boldsymbol{\sigma}_{(-i)i} = -(\mathbf{\Omega}_{(-i)(-i)}^{-1} \boldsymbol{\beta}) / \gamma$ ,  $\sigma_{ii} =$ 
|            $1/\gamma$ 
|           Save updated  $\mathbf{\Sigma}, \mathbf{T}, \mathbf{M}$ .
|       end for
|       Sample  $\tau, \xi$  as in (10). ▷ Sample  $\tau, \xi$ 
|   end for
|   Return MC samples  $\mathbf{\Omega}$ 
end function

```

desired posterior concentration results, we shall need to control both the actual dimension and the effective dimension of the true precision matrix. Overall, our theoretical analyses depend on certain assumptions on the true precision matrix, the dimension and sparsity, and the prior space. We present the details of these assumptions along with relevant discussions below.

Assumption 4.1. *The prior is restricted to a subspace of symmetric positive definite matrices, $\mathcal{M}_p^+(L)$, where*

$$\mathcal{M}_p^+(L) = \{\mathbf{\Omega} \in \mathcal{M}_p^+ : 0 < L^{-1} \leq \text{eig}_1(\mathbf{\Omega}) \leq \dots \leq \text{eig}_p(\mathbf{\Omega}) \leq L < \infty\}. \quad (11)$$

Assumption 4.2. *The actual dimension p satisfies the condition $p = n^b$, $b \in (0, 1)$, and the effective dimension $p + s$ satisfies $(p + s) \log p / n = o(1)$.*

Assumption 4.3. *The true precision matrix $\mathbf{\Omega}_0$ belongs to the parameter space given by*

$$\mathcal{U}(\varepsilon_0, s) = \{\mathbf{\Omega} \in \mathcal{M}_p^+ : \sum_{1 \leq i < j \leq p} \mathbb{1}(\omega_{ij} \neq 0) \leq s, 0 < \varepsilon_0^{-1} \leq \text{eig}_1(\mathbf{\Omega}) \leq \dots \leq \text{eig}_p(\mathbf{\Omega}) \leq \varepsilon_0 < \infty\}.$$

Assumption 4.4. The bound $[L^{-1}, L]$ on the eigenvalues of Ω as specified in (11) satisfies $L > \varepsilon_0$, or, in other words, $\varepsilon_0 = cL$, for some $c \in (0, 1)$.

Assumption 4.5. The global shrinkage parameter a satisfies the condition, $a^{1/2} < n^{-1/2}p^{-b_1}$, for some constant $b_1 > 0$.

The condition on the eigenvalues of Ω as specified in Assumption 4.1 is necessary for arriving at the theoretical results involving the posterior convergence rate of Ω . In this paper, we assume that L is a fixed constant, which can be large. However, this condition does not affect the practical implementation of our proposed method, and is used purely as a technical requirement, so that we only can work with Ω and Σ that are away from singular matrices. Beyond this, no structural assumptions such as decomposability are placed on either Ω or Σ . Similar assumptions have been made in related works; see Liu and Martin (2019) and Lee et al. (2021). Assumption 4.2 implies that the dimension grows to infinity as the sample size $n \rightarrow \infty$, but at a slower rate than n . Additionally, the condition on the effective dimension ensures that the posterior convergence rate goes to zero as $n \rightarrow \infty$. Similar conditions are necessary in proving the contraction results in other related works, for example, see Banerjee and Ghosal (2015); Lee et al. (2021); Liu and Martin (2019). Assumption 4.3 implies that the true precision matrix Ω_0 is sparse, and has eigenvalues that are bounded away from zero or infinity. Similar conditions are common in the literature on large precision matrix estimation problems; see, for example, Banerjee and Ghosal (2014, 2015); Lee et al. (2021); Liu and Martin (2019); among others. Assumption 4.4 is crucial in learning the precision matrix in a high-dimensional framework. This condition ensures that $\Omega_0 \in \mathcal{M}_p^+(L)$, that is, the prior space contains the true precision matrix, which is necessary in efficient learning of the same. Assumption 4.5 ensures that the prior puts sufficient mass around the true zero elements in the precision matrix. The condition on the global scale parameter a is a sufficient one, and is required to obtain the desired posterior convergence rate. We present the main theoretical result for posterior convergence now. A proof can be found in Appendix A.1.

Theorem 4.6. Let $\mathbf{X}^{(n)} = (\mathbf{X}_1, \dots, \mathbf{X}_n)^T$ be a random sample from a p -dimensional normal distribution with mean $\mathbf{0}$ and covariance matrix $\Sigma_0 = \Omega_0^{-1}$, where $\Omega_0 \in \mathcal{U}(\varepsilon_0, s)$. Consider the prior specification as given by (3). Under the assumptions on the prior as given in Assumptions (4.1)–(4.5), the posterior distribution of Ω satisfies

$$\mathbb{E}_0 \left[\Pr\{\|\Omega - \Omega_0\|_2 > M\epsilon_n \mid \mathbf{X}^{(n)}\} \right] \rightarrow 0,$$

for $\epsilon_n = n^{-1/2}(p + s)^{1/2}(\log p)^{1/2}$ and a sufficiently large constant $M > 0$.

Corollary 4.7. *Under similar conditions as in Theorem 4.6 above, the posterior distribution of Ω has the posterior convergence rate $\epsilon_n = n^{-1/2}(p + s)^{1/2}(\log p)^{1/2}$ around Ω_0 with respect to the Frobenius norm under the graphical horseshoe prior as specified in (5).*

A proof of Corollary 4.7 is in Supplementary Section S.4 and settles the question of posterior concentration for the graphical horseshoe which Li et al. (2019) did not address. The posterior convergence rate above directly compares with the rate of convergence of the frequentist graphical lasso estimator (Rothman et al., 2008), and is identical to the posterior convergence rates obtained by Banerjee and Ghosal (2015) and Liu and Martin (2019). However, our work is the first to address *unstructured precision matrices*, apart of a mild assumption of sparsity, using computationally efficient *continuous shrinkage priors*. This is at a contrast with previous theoretical analyses that imposed restrictive assumptions such as decomposability.

4.2 Properties of the MAP Estimator

The MAP estimator of Ω can be found by maximizing the following objective function:

$$\begin{aligned} Q(\Omega) = \log \pi(\Omega \mid \mathbf{X}^{(n)}) &= \ell(\Omega) + \sum_{i,j:i < j} \log \pi(\omega_{ij} \mid a) + C \\ &= \frac{n}{2} (\log \det \Omega - \text{tr}(\mathbf{S}\Omega)) - \sum_{i,j:i < j} \text{pen}_a(\omega_{ij}) + C, \end{aligned} \quad (12)$$

where, $\text{pen}_a(\omega) = -\log \log(1 + a/\omega^2)$, $a > 0$, is the horseshoe-like penalty. We start by proving $\text{pen}_a(\omega)$ is strictly concave in the following lemma, with a proof in Supplementary Section S.5.

Lemma 4.8. *The extended real-valued penalty function $\text{pen}_a(x) = -\log \log(1 + a/x^2)$, $a > 0$, is strictly concave for all $x \in \text{dom}(\text{pen}_a)$, separately for $x > 0$ and $x < 0$.*

A direct consequence of Lemma 4.8 is as follows. Let $\Omega^{(t)}$ be the t th iterate of a local linear approximation (LLA) algorithm (Zou and Li, 2008), that is,

$$\Omega^{(t+1)} = \text{argmax} \left\{ \ell(\Omega) - \sum_{i,j:i < j} \text{pen}'_a(|\omega_{ij}^{(t)}|) |\omega_{ij}| \right\}, \quad t = 1, 2, \dots$$

Then Theorem 1 of Zou and Li (2008), together with the strict concavity of horseshoe-like penalty function from Lemma 4.8, guarantees that the LLA algorithm will satisfy an ascent property, that is, $Q(\Omega^{(t+1)}) > Q(\Omega^{(t)})$, and hence the LLA algorithm will be a special case of minorize–maximize algorithms. We now present the result on consistency of the MAP estimate using the graphical horseshoe-like prior via an ECM algorithm, with a proof in Appendix A.2.

Theorem 4.9. *Under the conditions of Theorem 4.6, the MAP estimator of Ω , given by $\hat{\Omega}^{\text{MAP}}$ is consistent, in the sense that*

$$\|\hat{\Omega}^{\text{MAP}} - \Omega_0\|_2 = O_P(\epsilon_n),$$

where ϵ_n is the posterior convergence rate as defined in Theorem 4.6.

The above result guarantees that the MAP estimator also converges to the true precision matrix Ω_0 at the same rate as the posterior convergence rate in the Frobenius norm. By triangle inequality, Theorem 4.6 and Theorem 4.9 together imply that $\|\Omega - \hat{\Omega}^{\text{MAP}}\|_2 = O_P(\epsilon_n)$, so that the posterior probability of an ϵ_n -neighborhood around the MAP estimator with respect to the Frobenius norm converges to zero. This pleasing correspondence between the fully Bayesian and MAP estimates under the same prior-penalty dual is far from guaranteed, in the face of possible contradictions pointed out by [Castillo et al. \(2015\)](#) for the lasso in linear models.

5 Numerical Experiments

We compare the MAP and MCMC estimates under the horseshoe-based methods (GHS, GHS-LIKE-MCMC and GHS-LIKE-ECM) with two frequentist approaches: GLASSO, GSCAD and one Bayesian approach: the Bayesian GLASSO (BGL). We consider two problem dimensions: $(n, p) = (120, 100)$ and $(120, 200)$. For each dimension, we perform simulations under four different structures of the true precision matrix Ω_0 as in [Li et al. \(2019\)](#) and [Friedman et al. \(2008\)](#). These are: Random, Hubs, Cliques positive and Cliques negative, as detailed below.

1. *Random.* The off-diagonal entries of Ω_0 are non-zero with probability 0.01 when $p = 100$ and 0.002 when $p = 200$. The non-zero entries are then sampled uniformly from $(-1, -0.2)$.
2. *Hubs.* The rows/columns are partitioned into K disjoint groups G_1, \dots, G_K . The off-diagonal entries ω_{ij}^0 are set to 0.25 if $i \neq j$ and $i, j \in G_k$ for $k = 1, \dots, K$. In our simulations we consider $p/10$ groups with equal number of elements in each group.
3. *Cliques positive and Cliques negative.* Same as Hubs, except for setting all ω_{ij}^0 , $i \neq j$ and $i, j \in G_k$, we select 3 members within each group, $g_k \subset G_k$, and set $\omega_{ij}^0 = 0.75$, $i \neq j$ and $i, j \in g_k$ for ‘Cliques positive’ and set $\omega_{ij}^0 = -0.45$, $i \neq j$ and $i, j \in g_k$ for ‘Cliques negative.’

For each setting of (n, p) and Ω_0 , we generate 50 data sets and estimate the precision matrices by the methods stated above. All three horseshoe based methods are implemented in MATLAB, GSCAD is as implemented by [Wang \(2012\)](#) and GLASSO is implemented in R package ‘glasso’

(Friedman et al., 2018). Starting points for GHS-LIKE-ECM are randomly chosen in order to avoid getting stuck in a local minimum (see details in Supplementary Section S.7) and its global shrinkage parameter is chosen as in Supplementary Section S.6. Tuning parameters for GLASSO and GSCAD are chosen by 5-fold cross validation. The middle 50% posterior credible intervals are used for variable selection for the Bayesian approaches. We provide results on: Stein’s loss ($= \text{tr}(\hat{\Omega}\Sigma_0) - \log \det(\hat{\Omega}\Sigma_0) - p$), Frobenius norm (F norm $= \|\hat{\Omega} - \Omega_0\|_2$), true and false positive rates for detecting non-zero off-diagonal entries (resp., TPR and FPR), the Matthews Correlation Coefficient (MCC), and average CPU time. Note that for the fully Bayesian estimate, our theory concerns posterior concentration properties, and connections with convergence in Frobenius norm is established in Banerjee and Ghosal (2015). However, for the sake of completeness and comparisons with point estimation approaches, we provide variable selection results for all approaches as well, in addition to Stein’s loss (an empirical measure of Kullback–Leibler divergence) and F norm that focus more directly on the entire distribution.

It can be clearly seen from Tables 1–4 that the horseshoe based methods generally perform the best. GHS has the smallest Stein’s loss in all settings except in Hubs when $(n, p) = (120, 100)$. This corroborates the finding of Li et al. (2019) that GHS results in improved Kullback–Leibler risk properties (of which Stein’s loss is an empirical measure) when compared to prior densities that are bounded above at the origin, e.g., BGL, and it is apparent from both tables that BGL has the worst Stein’s loss. For GHS-LIKE-ECM and MCMC, the measures of Stein’s loss are generally close to that of GHS, and much better compared to the other competing methods. A similar pattern emerges in the results for F norm, with the horseshoe-based methods once again outperforming the competitors and performing similarly among themselves. It is worth noting, however, that the fully Bayesian approaches (GHS-LIKE-MCMC and GHS) generally result in the best statistical performance, at the expense of a considerably longer computing time, making the trade-off between fully Bayesian and penalized likelihood approaches apparent.

Coming next to variable selection results, one may expect the penalized likelihood approaches to really shine; since these methods produce exact zeros, unlike the Bayesian approaches that necessitate some form of post-processing. Nevertheless, the Bayesian approaches offer the advantage of controlling the trade-off between TPR and FPR, by varying the width of the credible interval, for example. With our chosen mechanism (i.e., a variable is considered not to be selected if the middle 50% credible interval includes zero), the GHS-LIKE-MCMC and GHS have the smallest TPR. Nevertheless, the penalized methods also have higher FPR in general (except for GHS-LIKE-ECM), which results in lower MCC overall. In particular, the GSCAD estimate,

Table 1: Mean (sd) Stein’s loss, Frobenius norm, true positive rates and false positive rates, Matthews Correlation Coefficient of precision matrix estimates over 50 data sets generated by multivariate normal distributions with precision matrix Ω_0 , where $n = 120$ and $p = 100$. The precision matrix is estimated by frequentist graphical lasso with penalized diagonal elements (GL1) and with unpenalized diagonal elements (GL2), graphical SCAD (GSCAD), Bayesian graphical lasso (BGL), the graphical horseshoe (GHS), graphical horseshoe-like ECM (ECM) and graphical horseshoe-like MCMC (MCMC). The best performer in each row is shown in bold. Average CPU time is in seconds.

Random 35 nonzero pairs out of 4950 nonzero elements $\sim -\text{Unif}(0.2, 1)$							
	GL1	GL2	GSCAD	BGL	GHS	ECM	MCMC
Stein’s loss	5.245 (0.254)	6.785 (0.464)	5.21 (0.242)	42.997 (0.898)	2.176 (0.278)	3.758 (0.282)	2.626 (0.317)
F norm	3.348 (0.115)	4.084 (0.143)	3.333 (0.117)	3.952 (0.139)	1.194 (0.144)	2.224 (0.108)	2.164 (0.16)
TPR	0.951 (0.03)	0.882 (0.038)	0.998 (0.009)	0.979 (0.023)	0.819 (0.041)	0.948 (0.032)	0.856 (0.036)
FPR	0.101 (0.013)	0.045 (0.007)	0.994 (0.005)	0.166 (0.0007)	0.0005 (0.0003)	0.071 (0.005)	0.003 (0.001)
MCC	0.232 (0.018)	0.321 (0.024)	0.005 (0.001)	0.181 (0.007)	0.869 (0.031)	0.275 (0.016)	0.776 (0.034)
Avg CPU time	4.988	4.719	53.977	550.422	252.84	5.94	538.929
Cliques negative 30 nonzero pairs out of 4950 nonzero elements = -0.45							
	GL1	GL2	GSCAD	BGL	GHS	ECM	MCMC
Stein’s loss	4.607 (0.223)	7.134 (0.529)	4.567 (0.231)	42.618 (0.896)	1.862 (0.263)	3.417 (0.251)	2.334 (0.307)
F norm	2.823 (0.117)	3.851 (0.138)	2.813 (0.112)	3.814 (0.165)	1.969 (0.212)	2.107 (0.124)	2.132 (0.199)
TPR	1 (0)	1 (0)	1 (0)	1 (0)	0.983 (.024)	1 (0)	0.988 (0.02)
FPR	0.1 (0.01)	0.028 (0.006)	0.983 (0.013)	0.158 (0.007)	0.0004 (0.0003)	0.073 (0.005)	0.002 (0.001)
MCC	0.232 (0.014)	0.42 (0.036)	0.01 (0.003)	0.177 (0.005)	0.936 (0.024)	0.268 (0.009)	0.843 (0.037)
Avg CPU time	2.962	3.2648	24.792	550.768	253.04	5.282	540.928

which is not guaranteed to be positive definite in finite samples (Fan et al., 2016), seems not to work well in general. Additional numerical results investigating the choice of starting values for the GHS-LIKE-ECM algorithm is given in Supplementary Section S.7.

6 Protein–Protein Interaction Network in B-cell Lymphoma

We analyze Reverse Phase Protein Array (RPPA) data of 33 patients with lymphoid neoplasm “Diffuse Large B-cell Lymphoma” to infer the protein interaction network. The data set consists

Table 2: Mean (sd) Stein’s loss, Frobenius norm, true positive rates and false positive rates, Matthews Correlation Coefficient of precision matrix estimates over 50 data sets generated by multivariate normal distributions with precision matrix Ω_0 , where $n = 120$ and $p = 100$. The precision matrix is estimated by frequentist graphical lasso with penalized diagonal elements (GL1) and with unpenalized diagonal elements (GL2), graphical SCAD (GSCAD), Bayesian graphical lasso (BGL), the graphical horseshoe (GHS), graphical horseshoe-like ECM (ECM) and graphical horseshoe-like MCMC (MCMC). The best performer in each row is shown in bold. Average CPU time is in seconds.

	Hubs						
	90 nonzero pairs out of 4950 nonzero elements = 0.25						
	GL1	GL2	GSCAD	BGL	GHS	ECM	MCMC
Stein’s loss	5.255 (0.263)	6.328 (0.414)	5.213 (0.261)	43.042 (0.802)	5.101 (0.455)	4.22 (0.369)	5.310 (0.485)
F norm	3.018 (0.091)	3.432 (0.112)	3.003 (0.093)	4.295 (0.156)	2.544 (0.126)	2.415 (0.103)	2.687 (0.141)
TPR	0.995 (0.007)	0.986 (0.017)	0.998 (0.002)	0.995 (0.008)	0.872 (0.04)	0.985 (0.014)	0.754 (0.004)
FPR	0.101 (0.016)	0.045 (0.008)	0.983 (0.012)	0.186 (0.007)	0.003 (0.001)	0.062 (0.005)	0.003 (0.001)
MCC	0.373 (0.027)	0.523 (0.039)	0.016 (0.006)	0.27 (0.006)	0.85 (0.027)	0.458 (0.015)	0.775 (0.033)
Avg CPU time	1.739	1.76	48.54	549.196	252.94	5.811	537.604
	Cliques positive						
	30 nonzero pairs out of 4950 nonzero elements = 0.75						
	GL1	GL2	GSCAD	BGL	GHS	ECM	MCMC
Stein’s loss	6.010 (0.212)	7.48 (0.45)	5.98 (0.21)	44.163 (0.790)	1.781 (0.232)	3.753 (0.275)	2.425 (0.323)
F norm	4.96 (0.1)	5.7 (0.13)	4.95 (0.107)	4.916 (0.103)	1.888 (0.184)	2.411 (0.142)	2.170 (0.198)
TPR	1 (0)	1 (0)	1 (0)	1 (0)	1 (0)	1 (0)	1 (0)
FPR	0.11 (0.013)	0.042 (0.0011)	0.972 (0.014)	0.177 (0.006)	0.0008 (0.005)	0.068 (0.006)	0.003 (0.001)
MCC	0.22 (0.013)	0.353 (0.041)	0.013 (0.003)	0.166 (0.004)	0.94 (0.031)	0.277 (0.012)	0.814 (0.035)
Avg CPU time	1.997	2.157	83.852	553.743	252.46	5.903	539.046

of protein expressions for 67 genes across 12 pathways for all patients. As in simulations, we use 50% posterior credible intervals for variable selection in GHS, BGL and GHS-LIKE-MCMC. The estimated sparsity (% of zero elements) and number of non zeros in the lower triangle of the estimates are given in Table 5. We note that the GHS-LIKE-MCMC gives the sparsest estimate, almost 4% sparser than the GHS. This is consistent with prior studies that found robust gene networks are typically sparse (Leclerc, 2008). As in the simulations, GSCAD performs the worst. To compare with a prior analysis of the same data set, we use the PRECISE framework of Ha et al. (2018). This method can infer directed edges, but we ignore the directionality since we are

Table 3: Mean (sd) Stein’s loss, Frobenius norm, true positive rates and false positive rates, Matthews Correlation Coefficient of precision matrix estimates over 50 data sets generated by multivariate normal distributions with precision matrix Ω_0 , where $n = 120$ and $p = 200$. The precision matrix is estimated by frequentist graphical lasso with penalized diagonal elements (GL1) and with unpenalized diagonal elements (GL2), graphical SCAD (GSCAD), Bayesian graphical lasso (BGL), the graphical horseshoe (GHS), graphical horseshoe-like ECM (ECM) and graphical horseshoe-like MCMC (MCMC). The best performer in each row is shown in bold. Average CPU time is in seconds.

Random 29 nonzero pairs out of 19900 nonzero elements $\sim -\text{Unif}(0.2, 1)$							
	GL1	GL2	GSCAD	BGL	GHS	ECM	MCMC
Stein’s loss	10.06 (0.4)	15.578 (1.12)	9.975 (0.4)	117.092 (1.563)	3.073 (0.305)	11.109 (0.562)	5.632 (0.523)
F norm	4.469 (0.151)	5.929 (0.176)	4.44 (0.156)	6.803 (0.162)	2.468 (0.137)	3.917 (0.108)	3.313 (0.178)
TPR	0.944 (0.036)	0.845 (0.036)	0.999 (0.005)	0.982 (0.024)	0.848 (0.038)	0.97 (0.028)	0.877 (0.041)
FPR	0.052 (0.007)	0.163 (0.002)	0.984 (0.011)	0.103 (0.003)	0.0001 (0.00007)	0.066 (0.003)	0.002 (0)
MCC	0.152 (0.011)	0.242 (0.015)	0.004 (0.002)	0.11 (0.004)	0.882 (0.029)	0.138 (0.005)	0.599 (0.035)
Avg CPU time	38.759	43.486	510.703	4484.22	1866.47	80.939	2260.3
Cliques negative 60 nonzero pairs out of 19900 nonzero elements = -0.45							
	GL1	GL2	GSCAD	BGL	GHS	ECM	MCMC
Stein’s loss	11.604 (0.401)	18.088 (0.993)	11.541 (0.396)	125.138 (1.714)	3.985 (0.403)	12.467 (0.626)	6.179 (0.403)
F norm	4.443 (0.088)	6.024 (0.143)	4.439 (0.076)	6.299 (0.168)	2.861 (0.209)	3.8 (0.126)	3.331 (0.2)
TPR	1 (0)	1 (0)	1 (0)	1 (0)	.975 (.173)	1 (0)	0.991 (0.012)
FPR	0.066 (0.004)	0.016 (0.002)	0.998 (0.005)	0.099 (0.002)	0.0002 (0.0001)	0.084 (0.003)	0.002 (0)
MCC	0.202 (0.006)	0.395 (0.027)	0.006 (0.001)	0.164 (0.002)	0.944 (0.16)	0.178 (0.003)	0.784 (0.028)
Avg CPU time	32.936	36.49	548.26	4492.67	1876.96	70.683	2249.3

interested in interactions and not causation. The proportions of edges in the estimates that ‘agree’ and ‘do not agree’ with the edges inferred using PRECISE framework are presented in Table 6. Protein networks realized from the estimates are presented in Figure 2. It can be seen that the GHS-LIKE-MCMC has the sparsest estimate among the methods that allow for interaction across all proteins, unlike the PRECISE framework that ignores interactions among proteins in different pathways, which may not be biologically justifiable.

Table 4: Mean (sd) Stein’s loss, Frobenius norm, true positive rates and false positive rates, Matthews Correlation Coefficient of precision matrix estimates over 50 data sets generated by multivariate normal distributions with precision matrix Ω_0 , where $n = 120$ and $p = 200$. The precision matrix is estimated by frequentist graphical lasso with penalized diagonal elements (GL1) and with unpenalized diagonal elements (GL2), graphical SCAD (GSCAD), Bayesian graphical lasso (BGL), the graphical horseshoe (GHS), graphical horseshoe-like ECM (ECM) and graphical horseshoe-like MCMC (MCMC). The best performer in each row is shown in bold. Average CPU time is in seconds.

	Hubs						
	180 nonzero pairs out of 19900						
	nonzero elements = 0.25						
	GL1	GL2	GSCAD	BGL	GHS	ECM	MCMC
Stein’s loss	12.407 (0.491)	15.243 (0.819)	12.331 (0.465)	123 (1.31)	11.692 (0.781)	12.825 (0.623)	12.741 (0.922)
F norm	4.594 (0.01)	5.3 (0.152)	4.583 (0.084)	7.129 (0.16)	3.763 (0.132)	4.209 (0.107)	4.179 (0.174)
TPR	0.99 (0.007)	0.976 (0.137)	1 (0)	0.991 (0.006)	0.779 (0.034)	0.986 (0.009)	0.737 (0.033)
FPR	0.065 (0.005)	0.024 (0.006)	0.999 (0.001)	0.119 (0.003)	0.001 (0.0003)	0.066 (0.003)	0.003 (0)
MCC	0.336 (0.015)	0.515 (0.043)	0.01 (0.003)	0.248 (0.003)	0.82 (0.024)	0.332 (0.006)	0.722 (0.03)
Avg CPU time	17.847	19.917	517.33	4499.30	1870.57	74.808	2523.1
	Cliques positive						
	60 nonzero pairs out of 19900						
	nonzero elements = 0.75						
	GL1	GL2	GSCAD	BGL	GHS	ECM	MCMC
Stein’s loss	14.523 (0.339)	17.262 (0.692)	14.477 (0.333)	126.487 (1.41)	3.797 (0.35)	13.512 (0.522)	6.717 (0.479)
F norm	7.59 (0.1)	8.553 (0.115)	7.596 (0.091)	7.936 (0.109)	2.733 (0.181)	4.248 (0.142)	3.535 (0.191)
TPR	1 (0)	1 (0)	1 (0)	1 (0)	1 (0)	1 (0)	1 (0)
FPR	0.065 (0.005)	0.024 (0.004)	0.991 (0.007)	0.115 (0.002)	0.0004 (0.0001)	0.08 (0.002)	0.003 (0)
MCC	0.205 (0.007)	0.335 (0.028)	0.01 (0.002)	0.15 (0.002)	0.959 (0.19)	0.184 (0.003)	0.735 (0.024)
Avg CPU time	23.768	25.3	880.46	4497.97	1872.55	80.652	2262.6

Table 5: Percentage of zeros (% Sparsity) and number of non-zero entries (NNZ) in the lower triangle of the precision matrix estimate of RPPA data for the competing approaches.

	MCMC	ECM	GHS	BGL	GL1	GL2	GSCAD
% Sparsity	95.79	88.6	91.59	73.72	69.88	73.67	9.06×10^{-4}
NNZ	93	252	186	581	666	582	2209

7 Concluding Remarks

Our main contribution in this paper is twofold: first, we propose a fully analytical prior-penalty dual termed the *graphical horseshoe-like* for inference in graphical models, and second, we provide

Table 6: Proportion of edges that ‘agree’ (AE) and ‘do not agree’ (NE) with the edges inferred using the PRECISE framework.

	MCMC	ECM	GHS	BGL	GL1	GL2	GSCAD
AE	0.238	0.412	0.325	0.575	0.638	0.6	1
NE	0.034	0.101	0.074	0.247	0.284	0.247	0.984

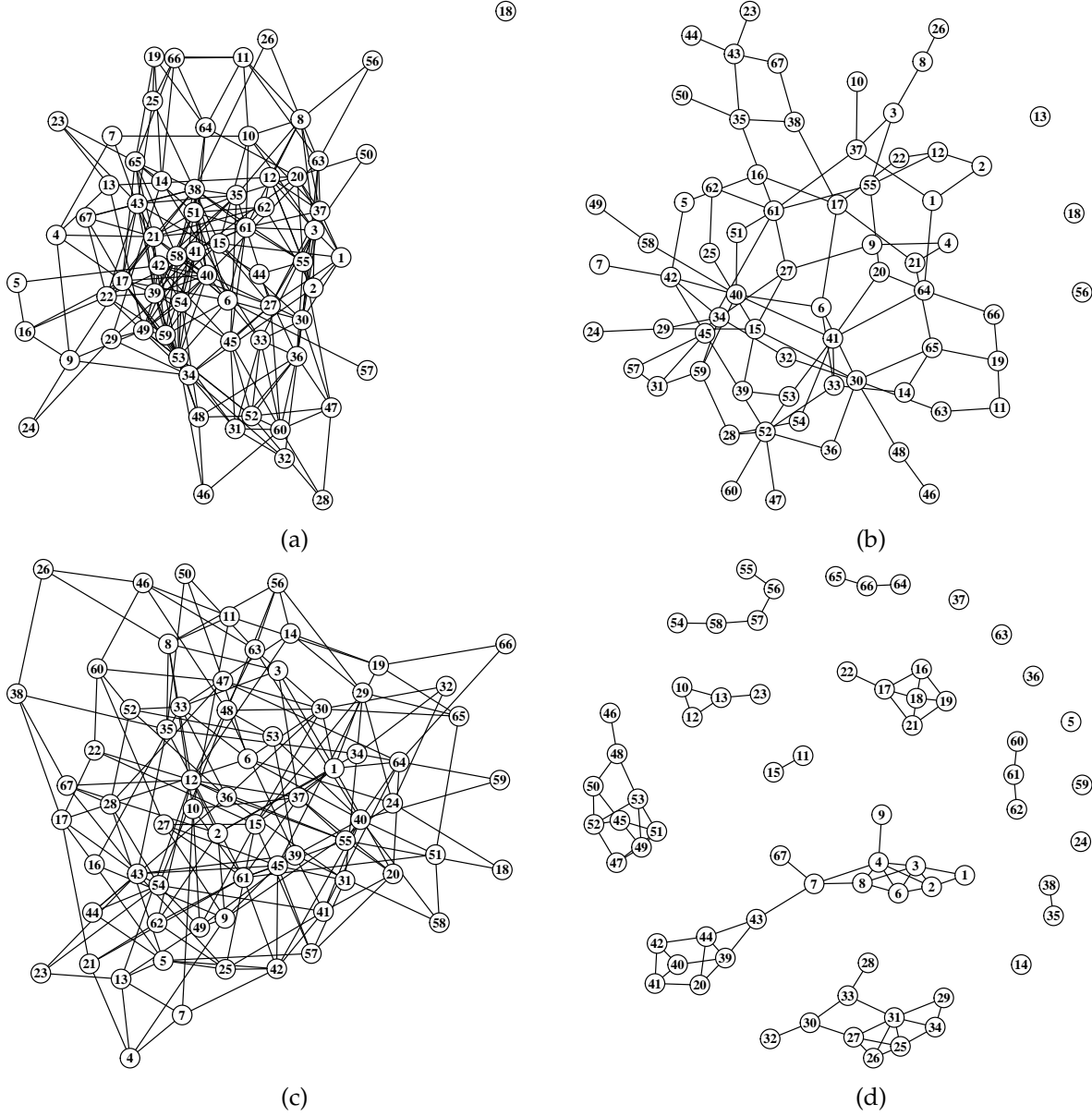


Figure 2: (a), (b), (c) and (d) correspond to RPPA networks for GHS-LIKE-ECM, GHS-LIKE-MCMC, GHS and PRECISE. The nodes are numbered from 1 to 67, which are proteins. The map between node numbers and protein names is given in the Supplementary Table S.2.

the first ever optimality results for both the frequentist point estimate as well as the fully Bayesian posterior. Consequently, we also establish the first Bayesian optimality results for the graphical horseshoe prior of [Li et al. \(2019\)](#). Our simulation studies clearly establish that the family of horseshoe based priors perform the best among state-of-the-art competitors across a wide range of data generating mechanisms, and suggest a potential trade-off between computational burden and statistical performance vis-à-vis penalized likelihood and fully Bayesian procedures. Our analysis of the RPPA data establishes the proposed approach as an effective regularizer of a gene interaction network; useful for identifying the key interactions in the disease etiology of cancer.

Although we focus on the estimation of Ω , two other important aspects of network inference are edge selection and the associated uncertainty quantification. Here we use posterior credible intervals for edge selection, but it might be interesting to incorporate other methods that have been proposed for variable selection with shrinkage priors, such as 2-means ([Bhattacharya et al., 2015](#)) or shrinkage factor thresholding ([Tang et al., 2018](#)), with appropriate modifications. On a related note, it will be interesting to establish the Bayes risk and the oracle under 0 – 1 loss and we conjecture that global-local shrinkage priors will attain such oracular risk with suitable assumptions on the prior tails and the global shrinkage parameter. Finally, it will be worth investigating whether one can extend the methods for generalized linear models, e.g. graphical models with exponential families as node-conditional distributions ([Yang et al., 2012](#)). It has been shown that while restricting the response distribution to natural exponential families with quadratic variance functions, shrinkage estimators enjoy certain optimality properties ([Xie et al., 2016](#)), and it remains to be settled whether similar properties hold true for graphical models as well.

Appendix

A.1 Proof of Theorem 4.6

We use the general theory of posterior convergence rate as outlined in Theorem 2.1 of [Ghosal et al. \(2000\)](#). We also refer to several auxiliary lemmas from Supplementary Section S.3 throughout the proof. We need to show the following:

- (i) the prior concentration rate of Kullback–Leibler ϵ_n^2 -neighborhoods is at least $\exp(-c n \epsilon_n^2)$ for some constant $c > 0$,
- (ii) for a suitably chosen sieve of densities \mathcal{P}_n , the ϵ_n -metric entropy of \mathcal{P}_n is bounded by a constant multiple of $n \epsilon_n^2$,

(iii) the probability of the complement of the above sieve is exponentially small, that is, $\Pi(\mathcal{P}_n^c) \leq \exp(-c'n\epsilon_n^2)$, for some constant $c' > 0$.

The above three parts together give the posterior convergence rate ϵ_n with respect to the Hellinger distance on the space of densities of the precision matrix. Owing to the intrinsic relationship between the Hellinger distance and the Frobenius distance for precision matrices as given by Lemma A.1 of [Banerjee and Ghosal \(2015\)](#), we get the desired posterior convergence rate.

(i) Prior concentration.

We first define $\mathcal{B}(p_{\Omega_0}, \epsilon_n)$, the ϵ_n^2 -neighborhoods of the true density in the Kullback–Leibler sense. For $K(p_1, p_2) = \int p_1 \log(p_1/p_2)$, $V(p_1, p_2) = \int p_1 \log^2(p_1/p_2)$, this is defined as $\mathcal{B}(p_{\Omega_0}, \epsilon_n) = \{p_{\Omega}: K(p_{\Omega_0}, p_{\Omega}) \leq \epsilon_n^2, V(p_{\Omega_0}, p_{\Omega}) \leq \epsilon_n^2\}$. For $\Omega_0 \in \mathcal{U}(\varepsilon_0, s)$, $\Omega \in \mathcal{M}_p^+(L)$, let d_1, \dots, d_p denote the eigenvalues of $\Omega_0^{-1/2}\Omega\Omega_0^{-1/2}$. Then, using Lemma S.3.1, we have,

$$\begin{aligned} K(p_{\Omega_0}, p_{\Omega}) &= -\frac{1}{2} \sum_{i=1}^p \log d_i - \frac{1}{2} \sum_{i=1}^n (1 - d_i), \\ V(p_{\Omega_0}, p_{\Omega}) &= \frac{1}{2} \sum_{i=1}^n (1 - d_i)^2 + K(p_{\Omega_0}, p_{\Omega})^2. \end{aligned} \quad (13)$$

Note that $\sum_{i=1}^n (1 - d_i)^2 = \|\mathbf{I}_p - \Omega_0^{-1/2}\Omega\Omega_0^{-1/2}\|_2^2$, so that, when $\|\mathbf{I}_p - \Omega_0^{-1/2}\Omega\Omega_0^{-1/2}\|_2^2$ is small, we have, $\max_{1 \leq i \leq p} |1 - d_i| < 1$. This gives, using (13),

$$K(p_{\Omega_0}, p_{\Omega}) = -\frac{1}{2} \sum_{i=1}^p \log d_i - \frac{1}{2} \sum_{i=1}^n (1 - d_i) \lesssim \sum_{i=1}^n (1 - d_i)^2, \quad V(p_{\Omega_0}, p_{\Omega}) \lesssim \sum_{i=1}^n (1 - d_i)^2.$$

Observe that,

$$\begin{aligned} \sum_{i=1}^n (1 - d_i)^2 &= \|\mathbf{I}_p - \Omega_0^{-1/2}\Omega\Omega_0^{-1/2}\|_2^2 = \|\Omega_0^{-1/2}(\Omega - \Omega_0)\Omega_0^{-1/2}\|_2^2 \\ &\leq \|\Omega_0^{-1}\|_2^2 \|\Omega - \Omega_0\|_2^2 \leq \varepsilon_0^{-2} \|\Omega - \Omega_0\|_2^2. \end{aligned}$$

Hence, for a sufficiently small constant $c_1 > 0$, we have,

$$\Pi(\mathcal{B}(p_0, \epsilon_n)) \geq \Pi\{\|\Omega - \Omega_0\|_2 \leq c_1 \epsilon_n\} \geq \Pi\{\|\Omega - \Omega_0\|_{\infty} \leq c_1 \epsilon_n/p\}.$$

The proposed prior on Ω has a bounded spectral norm. However, such a constraint can only increase the prior concentration, since $\Omega_0 \in \mathcal{U}(\varepsilon_0, s)$, $\varepsilon_0 < L$. Hence, we may pretend component-wise independence of the elements of Ω , so that the above expression can be simplified as products

of marginal prior probabilities. We have,

$$\begin{aligned} \Pi(\|\mathbf{\Omega} - \mathbf{\Omega}_0\|_\infty \leq c_1 \epsilon_n / p) &\gtrsim (c_1 \epsilon_n / p)^{(p+s)} \prod_{\{(i,j):\omega_{ij,0}=0\}} \pi(|\omega_{ij}| \leq c_1 \epsilon_n / p) \\ &\geq (c_1 \epsilon_n / p)^{(p+s)} \min_{\{(i,j):\omega_{ij,0}=0\}} \{\pi(|\omega_{ij}| \leq c_1 \epsilon_n / p)\}^{\binom{p}{2}-s}. \end{aligned}$$

Note that, from equation (S.4) in Lemma S.3.2, we have, for all $1 \leq i, j \leq p$,

$$\{\pi(|\omega_{ij}| \leq c_1 \epsilon_n / p)\}^{\binom{p}{2}-s} \geq \{1 - p^{-b'_1}\}^{\binom{p}{2}-s} \rightarrow 1.$$

Thus, $\Pi(\|\mathbf{\Omega} - \mathbf{\Omega}_0\|_\infty \leq c_1 \epsilon_n / p) \gtrsim (c_1 \epsilon_n / p)^{(p+s)}$. The prior concentration rate condition thus gives, $(p+s)(\log p + \log(1/\epsilon_n)) \asymp n \epsilon_n^2$, so as to yield $\epsilon_n = n^{-1/2}(p+s)^{1/2}(\log n)^{1/2}$.

(ii) Choosing the sieve and controlling metric entropy.

We now carefully choose a sieve in the space of prior densities to control its Hellinger metric entropy. Consider the sieve \mathcal{P}_n such that the maximum number of elements of $\mathbf{\Omega}$ exceeding $\delta_n = \epsilon_n / p^\nu$, $\nu > 0$ is at most \bar{r}_n , and the absolute values of the entries of $\mathbf{\Omega}$ are at most B . Formally, the sieve is thus given by,

$$\mathcal{P}_n = \{\mathbf{\Omega} \in \mathcal{M}_p^+(L) : \sum_{j,k} \mathbb{1}(|\omega_{jk}| > \delta_n) \leq \bar{r}_n, \|\mathbf{\Omega}\|_\infty \leq B\},$$

where $\delta_n = \epsilon_n / p^\nu$ and some sufficiently large $B > 0$. We shall choose B in such a way that the metric entropy condition is satisfied. Note that, for $\mathbf{\Omega}_1, \mathbf{\Omega}_2 \in \mathcal{M}_p^+(L)$, $\|\mathbf{\Omega}_1 - \mathbf{\Omega}_2\|_2^2 \leq p^2 \|\mathbf{\Omega}_1 - \mathbf{\Omega}_2\|_\infty^2$, so that, if $\|\mathbf{\Omega}_1 - \mathbf{\Omega}_2\|_\infty^2 \leq \epsilon_n^2 / p^{2\nu}$, where ν is such that $B \leq p^{\nu-1}$, we have, $\|\mathbf{\Omega}_1 - \mathbf{\Omega}_2\|_2^2 \leq \epsilon_n^2 / p^{2(\nu-1)}$.

The ϵ_n / p^ν -metric entropy w.r.t. the L_∞ -norm is given by

$$\begin{aligned} \log \left\{ \left(\frac{B p^\nu}{\epsilon_n} \right)^p \sum_{j=1}^{\bar{r}_n} \left(\frac{B p^\nu}{\epsilon_n} \right)^j \binom{\binom{p}{2}}{j} \right\} &= \log \left\{ \left(\frac{B p^\nu}{\epsilon_n} \right)^p \right\} + \log \left\{ \sum_{j=1}^{\bar{r}_n} \left(\frac{B p^\nu}{\epsilon_n} \right)^j \binom{\binom{p}{2}}{j} \right\} \\ &\leq \log \left\{ \left(\frac{B p^\nu}{\epsilon_n} \right)^p \right\} + \log \left\{ \bar{r}_n \left(\frac{B p^\nu}{\epsilon_n} \right)^{\bar{r}_n} \binom{p + \binom{p}{2}}{\bar{r}_n} \right\} \\ &\lesssim (\bar{r}_n + p)(\log p + \log B + \log(1/\epsilon_n)). \end{aligned}$$

Choosing $\bar{r}_n \sim k_1 n \epsilon_n^2 / \log n$, $k_1 > 0$, and $B \sim k_2 n \epsilon_n^2$, $k_2 > 0$, the above metric entropy is bounded by a constant multiple of $n \epsilon_n^2$. Since $\|\mathbf{\Omega}_1\|_{(2,2)} \leq p \|\mathbf{\Omega}_1\|_\infty \leq pB \leq p^\nu$, and $h^2(p_1, p_2) \leq p^2 \|\mathbf{\Omega}_1\|_{(2,2)}^2 \|\mathbf{\Omega}_1 - \mathbf{\Omega}_2\|_\infty^2$, the ϵ_n -metric entropy with respect to the Hellinger distance is also bounded by a constant multiple of $n \epsilon_n^2$. Thus, the rate ϵ_n obtained via the prior concentration rate calculation satisfies the metric entropy condition as well.

(iii) Controlling probability of the complement of the sieve.

The task of controlling the probability of the complement of the sieve can further be divided into two sub-parts. Note that,

$$\Pi(\mathcal{P}_n^c) \leq \Pi(N \geq \bar{r}_n + 1) + \Pi(\|\Omega\|_\infty > B).$$

We will calculate the probabilities in the right-hand side of the above display under an unconstrained case, and then take care of the truncation used in the prior for Ω , given by $\Omega \in \mathcal{M}_p^+(L)$, by finding a suitable lower bound for the event $\{0 < L^{-1} < \|\Omega\|_{(2,2)} < L < \infty\}$. Let us denote the prior under the unconstrained case by Π^* .

Define $N = \#\{(i, j): |\omega_{ij}| > \delta_n\}$. Note that, $N \sim \text{Bin}(p_n^*, \nu_n)$, $p_n^* = \binom{p}{2}$, $\nu_n = \Pr(|\omega_{ij}| > \delta_n)$. Using results on bounding the Binomial CDF as in [Song and Liang \(2017\)](#), we have,

$$\begin{aligned} \Pi^*(N \geq \bar{r}_n + 1) &\leq 1 - \Phi \left\{ (2p_n^* H[\nu_n, \bar{r}_n/p_n^*])^{1/2} \right\} \\ &\leq (2\pi)^{-1/2} (2p_n^* H[\nu_n, \bar{r}_n/p_n^*])^{-1/2} \exp\{-p_n^* H[\nu_n, \bar{r}_n/p_n^*]\}, \end{aligned}$$

where

$$p_n^* H[\nu_n, \bar{r}_n/p_n^*] = \bar{r}_n \log \left(\frac{\bar{r}_n}{p_n^* \nu_n} \right) + (p_n^* - \bar{r}_n) \log \left(\frac{p_n^* - \bar{r}_n}{p_n^* - p_n^* \nu_n} \right).$$

It suffices to prove that $p_n^* H[\nu_n, \bar{r}_n/p_n^*] \geq O(n\epsilon_n^2)$. We have,

$$p_n^* H[\nu_n, \bar{r}_n/p_n^*] \approx \bar{r}_n \log \left(\frac{\bar{r}_n}{p_n \nu_n} \right) + (p_n^2 - \bar{r}_n) \log \left(\frac{p_n^2 - \bar{r}_n}{p_n^2 - p_n^2 \nu_n} \right).$$

For the first term on the RHS above, we have, $\bar{r}_n \log\{\bar{r}_n/(p_n \nu_n)\} \geq \bar{r}_n \log \bar{r}_n + b'_1 \bar{r}_n \log p_n$, since $\nu_n \leq p_n^{-b'_1}$ vide (S.4) in Lemma S.3.2. Note that $\bar{r}_n \log p \sim \bar{r}_n \log n \asymp n\epsilon_n^2$, so as to get $\bar{r}_n \log\{\bar{r}_n/(p_n \nu_n)\} \geq n\epsilon_n^2$. For the second term, we have, $(p_n^2 - \bar{r}_n) \log\{(p_n^2 - \bar{r}_n)/(p_n^2 - p_n^2 \nu_n)\} \asymp \bar{r}_n (1 - \bar{r}_n/p_n^2) = o(n\epsilon_n^2)$. Hence, we get, $p_n^* H[\nu_n, \bar{r}_n/p_n^*] \geq O(n\epsilon_n^2)$, which implies,

$$\Pi^*(N \geq \bar{r}_n + 1) \leq \exp\{-C' n\epsilon_n^2\}, \quad (14)$$

for some $C' > 0$. From (S.5) in Lemma S.3.2, for the choice of $B \sim k_2 n\epsilon_n^2$ as outlined in the metric entropy condition above, we have,

$$\Pi^*(\|\Omega\|_\infty > B) \leq 2p^2 \exp(-k_2 n\epsilon_n^2). \quad (15)$$

Combining equations (14) and (15), we get, for a suitable constant $c_3 > 0$,

$$\Pi^*(N \geq \bar{r}_n + 1) + \Pi^*(\|\mathbf{\Omega}\|_\infty > B) \lesssim \exp(-c_3 n \epsilon_n^2). \quad (16)$$

Combining (16) and (S.8), we get, for a suitable constant $c_4 > 0$,

$$\begin{aligned} \Pi(\mathcal{P}_n^c) &= \frac{\Pi^*(\mathcal{P}_n^c)}{\Pi(\mathbf{\Omega} \in \mathcal{M}_p^+(L))} \lesssim \exp(-c_3 n \epsilon_n^2) L^{-p} \exp(C_1 p n^{-1/2}) \\ &= \exp(-c_3 n \epsilon_n^2 - p \log L + C_2 p n^{-1/2}) \\ &\lesssim \exp(-c_4 n \epsilon_n^2). \end{aligned}$$

Hence, the complement of the chosen sieve has exponentially small prior probability. Thus, $\epsilon_n = n^{-1/2}(p + s)^{1/2}(\log n)^{1/2}$ is the posterior convergence rate and the result is established.

A.2 Proof of Theorem 4.9

Consider the MAP estimator of the precision matrix corresponding to the graphical horseshoe-like prior $\hat{\mathbf{\Omega}}^{\text{MAP}}$ as outlined in Section 4.2. Define $\mathbf{\Delta} = ((\delta_{ij})) = \mathbf{\Omega} - \mathbf{\Omega}_0$ such that $\|\mathbf{\Delta}\|_2 = M \epsilon_n$, $M > 0$ is a large constant. Here, $\mathbf{\Omega}_0 = ((\omega_{ij,0}))$ is the true precision matrix. The true covariance matrix is $\mathbf{\Sigma}_0 = ((\sigma_{ij,0}))$, and the natural estimator of the covariance is $\mathbf{S} = ((s_{ij}))$. Consider $Q(\mathbf{\Omega})$ as defined in (12). If we can show that for some small $\varepsilon > 0$,

$$\mathbb{P} \left(\sup_{\|\mathbf{\Delta}\|_2 = M \epsilon_n} Q(\mathbf{\Omega}_0 + \mathbf{\Delta}) < Q(\mathbf{\Omega}_0) \right) \geq 1 - \varepsilon,$$

then there exists a local maximizer $\hat{\mathbf{\Omega}}$ such that $\|\hat{\mathbf{\Omega}} - \mathbf{\Omega}_0\|_2 = O_P(\epsilon_n)$. We have,

$$\begin{aligned} Q(\mathbf{\Omega}) &= l(\mathbf{\Omega}) - \sum_{i < j} \text{pen}(\omega_{ij}) = \frac{n}{2} \log \det(\mathbf{\Omega}) - \frac{n}{2} \text{tr}(\mathbf{S}\mathbf{\Omega}) - \sum_{i < j} \text{pen}(\omega_{ij}) \\ &= \frac{n}{2} \left\{ \log \det(\mathbf{\Omega}) - \text{tr}(\mathbf{S}\mathbf{\Omega}) - \frac{2}{n} \sum_{i < j} \text{pen}(\omega_{ij}) \right\} = \frac{n}{2} h(\mathbf{\Omega}), \text{ say.} \end{aligned}$$

Let us denote as $(2/n) \text{pen}(\omega_{ij})$ as $p_n(\omega_{ij})$. This gives,

$$\begin{aligned} h(\mathbf{\Omega}_0 + \mathbf{\Delta}) - h(\mathbf{\Omega}) &= \log \det(\mathbf{\Omega}_0 + \mathbf{\Delta}) - \text{tr}(\mathbf{S}(\mathbf{\Omega}_0 + \mathbf{\Delta})) - \log \det(\mathbf{\Omega}_0) + \text{tr}(\mathbf{S}\mathbf{\Omega}_0) \\ &\quad - \sum_{i < j} \{p_n(\omega_{ij,0} + \delta_{ij}) - p_n(\omega_{ij,0})\}. \end{aligned} \quad (17)$$

By Taylor's series expansion of logarithm of the determinant of a matrix, we have,

$$\begin{aligned} & \log \det(\mathbf{\Omega}_0 + \mathbf{\Delta}) - \log \det(\mathbf{\Omega}_0) \\ = & \text{tr}(\mathbf{\Sigma}_0 \mathbf{\Delta}) - \text{vec}(\mathbf{\Delta})^T \left[\int_0^1 (1 - \nu)(\mathbf{\Omega}_0 + \nu \mathbf{\Delta})^{-1} \otimes (\mathbf{\Omega}_0 + \nu \mathbf{\Delta})^{-1} d\nu \right] \text{vec}(\mathbf{\Delta}). \end{aligned}$$

Plugging the above in (17), we have the expression for $h(\mathbf{\Omega}_0 + \mathbf{\Delta}) - h(\mathbf{\Omega})$ as

$$\begin{aligned} & \text{tr}[(\mathbf{\Sigma}_0 - \mathbf{S})\mathbf{\Delta}] - \text{vec}(\mathbf{\Delta})^T \left[\int_0^1 (1 - \nu)(\mathbf{\Omega}_0 + \nu \mathbf{\Delta})^{-1} \otimes (\mathbf{\Omega}_0 + \nu \mathbf{\Delta})^{-1} d\nu \right] \text{vec}(\mathbf{\Delta}) \\ & - \sum_{i < j} \{p_n(\omega_{ij,0} + \delta_{ij}) - p_n(\omega_{ij,0})\} \\ = & \text{I} + \text{II} + \text{III, say.} \end{aligned} \tag{18}$$

We shall now separately bound the three terms I, II, and III. For bounding I, we have,

$$|\text{tr}[(\mathbf{\Sigma}_0 - \mathbf{S})\mathbf{\Delta}]| \leq \left| \sum_{i \neq j} (\sigma_{ij,0} - s_{ij}) \delta_{ij} \right| + \left| \sum_i (\sigma_{ii,0} - s_{ii}) \delta_{ii} \right|. \tag{19}$$

Using Boole's inequality and Lemma S.3.7, we have, with probability tending to one,

$$\max_{i \neq j} |s_{ij} - \sigma_{ij,0}| \leq C_1 \left(\frac{\log p}{n} \right)^{1/2}.$$

Hence, the first term in the RHS of display (19) is bounded by $C_1 (\log p/n)^{1/2} \|\mathbf{\Delta}^-\|_1$. By Cauchy-Schwarz inequality and Lemma S.3.7, we have, with probability tending to one,

$$\begin{aligned} \left| \sum_i (\sigma_{ii,0} - s_{ii}) \delta_{ii} \right| & \leq \left\{ \sum_i (\sigma_{ii,0} - s_{ii})^2 \right\}^{1/2} \|\mathbf{\Delta}^+\|_2 \leq p^{1/2} \max_{1 \leq i \leq p} |s_{ii} - \sigma_{ii,0}| \|\mathbf{\Delta}^+\|_2 \\ & \leq C_2 \left(\frac{p \log p}{n} \right)^{1/2} \|\mathbf{\Delta}^+\|_2 \leq C_2 \left(\frac{(p+s) \log p}{n} \right)^{1/2} \|\mathbf{\Delta}^+\|_2. \end{aligned}$$

Thus, combining the bounds above, with probability approaching one, a bound for expression I is,

$$\text{I} \leq C_1 \left(\frac{\log p}{n} \right)^{1/2} \|\mathbf{\Delta}^-\|_1 + C_2 \left(\frac{(p+s) \log p}{n} \right)^{1/2} \|\mathbf{\Delta}^+\|_2. \tag{20}$$

Now we proceed to find suitable bounds for expression II. Note that II is upper bounded by the negative of the minimum of $\text{vec}(\mathbf{\Delta})^T \left[\int_0^1 (1 - \nu)(\mathbf{\Omega}_0 + \nu \mathbf{\Delta})^{-1} \otimes (\mathbf{\Omega}_0 + \nu \mathbf{\Delta})^{-1} d\nu \right] \text{vec}(\mathbf{\Delta})$.

Using the result that $\min_{\|x\|_2=1} x^T A x = \text{eig}_1(A)$, we have,

$$\begin{aligned}
& \min \left\{ \text{vec}(\Delta)^T \left[\int_0^1 (1-\nu)(\Omega_0 + \nu\Delta)^{-1} \otimes (\Omega_0 + \nu\Delta)^{-1} d\nu \right] \text{vec}(\Delta) \right\} \\
&= \|\Delta\|_2^2 \text{eig}_1 \left[\int_0^1 (1-\nu)(\Omega_0 + \nu\Delta)^{-1} \otimes (\Omega_0 + \nu\Delta)^{-1} d\nu \right] \\
&\geq \|\Delta\|_2^2 \int_0^1 (1-\nu) \text{eig}_1^2(\Omega_0 + \nu\Delta)^{-1} d\nu \geq \frac{1}{2} \|\Delta\|_2^2 \min_{0 \leq \nu \leq 1} \text{eig}_1^2(\Omega_0 + \nu\Delta)^{-1} \\
&\geq \frac{1}{2} \min \{ \text{eig}_1^2(\Omega_0 + \Delta)^{-1} : \|\Delta\|_2 \leq M\epsilon_n \}.
\end{aligned}$$

Note that, $\text{eig}_1^2(\Omega_0 + \Delta)^{-1} = \text{eig}_p^{-2}(\Omega_0 + \Delta) \geq (\|\Omega_0\|_{(2,2)} + \|\Delta\|_{(2,2)})^{-2} \geq \epsilon_0^2/2$, with probability tending to one. The last inequality follows from the fact that $\|\Delta\|_{(2,2)} \leq \|\Delta\|_2 = o(1)$. Hence, with probability tending to one, we have the bound for expression II as

$$\text{II} \leq -\frac{1}{4} \epsilon_0^2 \|\Delta\|_2^2. \quad (21)$$

Finally, we proceed to find suitable bounds for expression III. Let us denote the set $\mathcal{S} = \{(i, j) : \omega_{ij,0} = 0, i < j\}$. This set comprises of the indices in the upper triangle of the true precision matrix that are exactly equal to zero. The complement of \mathcal{S} consists of the indices with non-zero entries in the upper triangle of the same. We can partition expression III (without the negative sign) as

$$\begin{aligned}
\sum_{i < j} \{p_n(\omega_{ij,0} + \delta_{ij}) - p_n(\omega_{ij,0})\} &= \sum_{(i,j) \in \mathcal{S}} \{p_n(\omega_{ij,0} + \delta_{ij}) - p_n(\omega_{ij,0})\} + \sum_{(i,j) \in \mathcal{S}^c} \{p_n(\omega_{ij,0} + \delta_{ij}) - p_n(\omega_{ij,0})\} \\
&= \sum_{(i,j) \in \mathcal{S}} \{p_n(\delta_{ij}) - p_n(0)\} + \sum_{(i,j) \in \mathcal{S}^c} \{p_n(\omega_{ij,0} + \delta_{ij}) - p_n(\omega_{ij,0})\} \\
&> \frac{M'}{n} + \sum_{(i,j) \in \mathcal{S}^c} \{p_n(\omega_{ij,0} + \delta_{ij}) - p_n(\omega_{ij,0})\}.
\end{aligned}$$

The last inequality follows from the fact that $p_n(\theta) \rightarrow -\infty$ as $|\theta| \rightarrow 0$, and hence the first term in the above expression is larger than M'/n for some large $M' > 0$. This implies:

$$\sum_{i < j} \{p_n(\omega_{ij,0} + \delta_{ij}) - p_n(\omega_{ij,0})\} > \sum_{(i,j) \in \mathcal{S}^c} \{p_n(\omega_{ij,0} + \delta_{ij}) - p_n(\omega_{ij,0})\}.$$

By Taylor's series expansion of $p_n(\omega_{ij} + \delta_{ij})$ around $\omega_{ij,0} (\neq 0)$, we have,

$$p_n(\omega_{ij} + \delta_{ij}) - p_n(\omega_{ij,0}) = \delta_{ij} p_n'(\omega_{ij,0}) + \frac{1}{2} \delta_{ij}^2 p_n''(\omega_{ij,0})(1 + o(1)).$$

Since $-x \leq |x|$, we can write,

$$\begin{aligned}
& - \sum_{(i,j) \in \mathcal{S}^c} \{p_n(\omega_{ij,0} + \delta_{ij}) - p_n(\omega_{ij,0})\} \\
& \leq \max \{|p'_n(\omega_{ij,0})|\} \sum_{(i,j) \in \mathcal{S}^c} |\delta_{ij}| + \frac{1}{2} \max \{|p''_n(\omega_{ij,0})|\} \sum_{(i,j) \in \mathcal{S}^c} \delta_{ij}^2 (1 + o(1)) \\
& \leq \max \{|p'_n(\omega_{ij,0})|\} \|\Delta^{-1}\|_1 + \frac{1}{2} \max \{|p''_n(\omega_{ij,0})|\} \|\Delta^{-}\|_2^2 (1 + o(1)) \\
& \leq s^{1/2} \max \{|p'_n(\omega_{ij,0})|\} \|\Delta\|_2 + \frac{1}{2} \max \{|p''_n(\omega_{ij,0})|\} \|\Delta\|_2^2 (1 + o(1)). \tag{22}
\end{aligned}$$

Now, note that,

$$|p'_n(\omega_{ij,0})| = \frac{2}{n} |pen'(\omega_{ij,0})| = \frac{2}{n} \frac{2a/|\omega_{ij,0}|^3}{(1 + \frac{a}{\omega_{ij,0}^2}) \log \left(1 + \frac{a}{\omega_{ij,0}^2}\right)}.$$

Since $(1+x) \log(1+x) > x$ for $x > -1, x \neq 0$, we have, $|p'_n(\omega_{ij,0})| < 4/(n|\omega_{ij,0}|)$. We now arrive at a suitable bound for the double derivative of the penalty. Note that, for $\theta \neq 0$,

$$\begin{aligned}
pen''(\theta) &= - \frac{2a \left\{ (a + 3\theta^2) \log \left(1 + \frac{a}{\theta^2}\right) - 2a \right\}}{\theta^6 \left(1 + \frac{a}{\theta^2}\right)^2 \log^2 \left(1 + \frac{a}{\theta^2}\right)} \\
&\leq - \frac{2a \left\{ (a + 3\theta_0^2) \log \left(1 + \frac{a}{\theta_0^2}\right) - 2a \right\}}{\theta^6 \left(1 + \frac{a}{\theta^2}\right)^2 \log^2 \left(1 + \frac{a}{\theta^2}\right)},
\end{aligned}$$

where $\theta_0 = \arg \max_{\theta} \{-(a + 3\theta^2) \log(1 + a/\theta^2)\} = (ak)^{1/2}$, $k = \{\exp(z_0) - 1\}^{-1}$, $z_0 \approx 1.0356$. Hence,

$$\begin{aligned}
|pen''(\theta)| &\leq \frac{2a \left| (a + 3\theta_0^2) \log \left(1 + \frac{a}{\theta_0^2}\right) - 2a \right|}{\theta^6 \left(1 + \frac{a}{\theta^2}\right)^2 \log^2 \left(1 + \frac{a}{\theta^2}\right)} \\
&\leq \frac{2a \left| (a + 3\theta_0^2) \log \left(1 + \frac{a}{\theta_0^2}\right) - 2a \right|}{\theta^6 \frac{a^2}{\theta^4}} = \frac{2 \left| (a + 3\theta_0^2) \log \left(1 + \frac{a}{\theta_0^2}\right) - 2a \right|}{a\theta^2} \\
&= \frac{2 \left| (a + 3ak) \log \left(1 + \frac{a}{ak}\right) - 2a \right|}{a\theta^2} \approx \frac{C_3}{\theta^2},
\end{aligned}$$

where $C_3 > 0$ is a constant not depending on n or a . This gives,

$$|p_n''(\omega_{ij,0})| = \frac{2}{n} |pen''(\omega_{ij,0})| < \frac{2C_3}{n \min_{(i,j) \in \mathcal{S}^c} \omega_{ij,0}^2}.$$

Thus, expression III can be bounded as follows:

$$\text{III} \leq s^{1/2} \|\Delta\|_2 \frac{4}{n \min_{(i,j) \in \mathcal{S}^c} |\omega_{ij,0}|} + \frac{C_3}{n \min_{(i,j) \in \mathcal{S}^c} \omega_{ij,0}^2} \|\Delta\|_2^2 (1 + o(1)). \quad (23)$$

Combining Equations (20), (21), and (23), we have, with probability tending to one,

$$\begin{aligned} & Q(\Omega_0 + \Delta) - Q(\Omega_0) \\ \leq & C_1 \left(\frac{\log p}{n} \right)^{1/2} \|\Delta^-\|_1 + C_2 \left(\frac{(p+s) \log p}{n} \right)^{1/2} \|\Delta^+\|_2 - \frac{1}{4} \varepsilon_0^2 \|\Delta\|_2^2 \\ & + s^{1/2} \|\Delta\|_2 \frac{4}{n \min_{(i,j) \in \mathcal{S}^c} |\omega_{ij,0}|} + \frac{C_3}{n \min_{(i,j) \in \mathcal{S}^c} \omega_{ij,0}^2} \|\Delta\|_2^2 (1 + o(1)) \\ \leq & C_1 \left(\frac{(p+s) \log p}{n} \right)^{1/2} \|\Delta\|_2 + C_2 \left(\frac{(p+s) \log p}{n} \right)^{1/2} \|\Delta\|_2 - \frac{1}{4} \varepsilon_0^2 \|\Delta\|_2^2 \\ & + s^{1/2} \|\Delta\|_2 \frac{4}{n \min_{(i,j) \in \mathcal{S}^c} |\omega_{ij,0}|} + \frac{C_3}{n \min_{(i,j) \in \mathcal{S}^c} \omega_{ij,0}^2} \|\Delta\|_2^2 (1 + o(1)) \\ \leq & \|\Delta\|_2^2 \left\{ C_1 \left(\frac{(p+s) \log p}{n} \right)^{1/2} \|\Delta\|_2^{-1} + C_2 \left(\frac{(p+s) \log p}{n} \right)^{1/2} \|\Delta\|_2^{-1} - \frac{1}{4} \varepsilon_0^2 \right. \\ & \left. + (p+s)^{1/2} \|\Delta\|_2^{-1} \frac{4}{n \min_{(i,j) \in \mathcal{S}^c} |\omega_{ij,0}|} + \frac{C_3}{n \min_{(i,j) \in \mathcal{S}^c} \omega_{ij,0}^2} (1 + o(1)) \right\} \\ = & \|\Delta\|_2^2 \left\{ \frac{C_1}{M} + \frac{C_2}{M} - \frac{1}{4} \varepsilon_0^2 + \frac{4}{(n \log p)^{1/2} \min_{(i,j) \in \mathcal{S}^c} |\omega_{ij,0}|} + \frac{C_3}{n \min_{(i,j) \in \mathcal{S}^c} \omega_{ij,0}^2} (1 + o(1)) \right\} < 0, \end{aligned}$$

for M sufficiently large, and owing to the fact that the last two terms inside the bracket in the above display are $o(1)$ as $\min_{(i,j) \in \mathcal{S}^c} |\omega_{ij,0}|$ are bounded away from zero. This completes the proof.

SUPPLEMENTARY MATERIAL

Supplementary Material available online includes a summary of notations, additional details on the proposed prior, auxiliary lemmas used in the main theorems, and additional results on simulated and proteomics data. It also contains a computer code archive along with an instructional README file.

References

- Banerjee, S. and Ghosal, S. (2014). Posterior convergence rates for estimating large precision matrices using graphical models. *Electronic Journal of Statistics*, 8(2):2111–2137.
- Banerjee, S. and Ghosal, S. (2015). Bayesian structure learning in graphical models. *Journal of Multivariate Analysis*, 136:147–162.
- Barndorff-Nielsen, O., Kent, J., and Sørensen, M. (1982). Normal variance-mean mixtures and z distributions. *International Statistical Review*, pages 145–159.
- Bhadra, A., Datta, J., Polson, N. G., and Willard, B. (2016). Default Bayesian analysis with global-local shrinkage priors. *Biometrika*, 103(4):955–969.
- Bhadra, A., Datta, J., Polson, N. G., and Willard, B. (2017). The Horseshoe+ Estimator of Ultra-Sparse Signals. *Bayesian Analysis*, 12(4):1105–1131.
- Bhadra, A., Datta, J., Polson, N. G., and Willard, B. T. (2019a). The horseshoe-like regularization for feature subset selection. *Sankhya B*, pages 1–30.
- Bhadra, A., Datta, J., Polson, N. G., and Willard, B. T. (2019b). Lasso meets horseshoe: A survey. *Statistical Science*, 34(3):405–427.
- Bhattacharya, A., Pati, D., Pillai, N. S., and Dunson, D. B. (2015). Dirichlet–Laplace priors for optimal shrinkage. *Journal of the American Statistical Association*, 110(512):1479–1490.
- Bickel, P. J. and Levina, E. (2008). Regularized estimation of large covariance matrices. *The Annals of Statistics*, 36(1):199–227.
- Brualdi, R. A. and Mellendorf, S. (1994). Regions in the complex plane containing the eigenvalues of a matrix. *The American Mathematical Monthly*, 101(10):975–985.
- Cai, T., Liu, W., and Luo, X. (2011). A constrained ℓ_1 minimization approach to sparse precision matrix estimation. *Journal of the American Statistical Association*, 106(494):594–607.
- Callot, L., Caner, M., Önder, A. Ö., and Ulaşan, E. (2019). A nodewise regression approach to estimating large portfolios. *Journal of Business & Economic Statistics*, pages 1–12.
- Candès, E. J. and Tao, T. (2010). The power of convex relaxation: Near-optimal matrix completion. *IEEE Transactions on Information Theory*, 56(5):2053–2080.

- Carvalho, C. M., Polson, N. G., and Scott, J. G. (2010). The horseshoe estimator for sparse signals. *Biometrika*, 97(2):465–480.
- Castillo, I., Schmidt-Hieber, J., and van der Vaart, A. (2015). Bayesian linear regression with sparse priors. *The Annals of Statistics*, 43(5):1986–2018.
- Dawid, A. P., Stone, M., and Zidek, J. V. (1973). Marginalization paradoxes in Bayesian and structural inference. *Journal of the Royal Statistical Society: Series B*, 35(2):189–213.
- Fan, J., Feng, Y., and Wu, Y. (2009). Network exploration via the adaptive lasso and SCAD penalties. *The Annals of Applied Statistics*, 3(2):521–541.
- Fan, J. and Li, R. (2001). Variable selection via nonconcave penalized likelihood and its oracle properties. *Journal of the American Statistical Association*, 96(456):1348–1360.
- Fan, J., Liao, Y., and Liu, H. (2016). An overview of the estimation of large covariance and precision matrices. *The Econometrics Journal*, 19(1):C1–C32.
- Friedman, J., Hastie, T., and Tibshirani, R. (2008). Sparse inverse covariance estimation with the graphical lasso. *Biostatistics*, 9(3):432–441.
- Friedman, J., Hastie, T., and Tibshirani, R. (2018). *glasso: Graphical Lasso: Estimation of Gaussian Graphical Models*. R package version 1.10.
- Gan, L., Narisetty, N. N., and Liang, F. (2019). Bayesian regularization for graphical models with unequal shrinkage. *Journal of the American Statistical Association*, 114(527):1218–1231.
- Ghosal, S., Ghosh, J. K., and van der Vaart, A. W. (2000). Convergence rates of posterior distributions. *The Annals of Statistics*, 28(2):500–531.
- Ha, M. J., Banerjee, S., Akbani, R., Liang, H., Mills, G. B., Do, K.-A., and Baladandayuthapani, V. (2018). Personalized integrated network modeling of the cancer proteome atlas. *Scientific Reports*, 8(1):1–14.
- Huynh-Thu, V. A. and Sanguinetti, G. (2019). Gene regulatory network inference: an introductory survey. In *Gene Regulatory Networks*, pages 1–23. Springer.
- Kuismin, M. O., Kempainen, J. T., and Sillanpää, M. J. (2017). Precision matrix estimation with ROPE. *Journal of Computational and Graphical Statistics*, 26(3):682–694.

- Lam, C. and Fan, J. (2009). Sparsistency and rates of convergence in large covariance matrix estimation. *The Annals of Statistics*, 37(6B):4254.
- Lauritzen, S. L. (1996). *Graphical Models*. Oxford University Press.
- Leclerc, R. D. (2008). Survival of the sparsest: robust gene networks are parsimonious. *Molecular Systems Biology*, 4(1):213.
- Lee, K., Jo, S., and Lee, J. (2021). The beta-mixture shrinkage prior for sparse covariances with posterior minimax rates. *arXiv preprint arXiv:2101.04351*.
- Lee, K. and Lee, J. (2021). Estimating large precision matrices via modified Cholesky decomposition. *Statistica Sinica*, 31(2021):173–196.
- Li, Y., Craig, B. A., and Bhadra, A. (2019). The graphical horseshoe estimator for inverse covariance matrices. *Journal of Computational and Graphical Statistics*, 28(3):747–757.
- Liu, C. and Martin, R. (2019). An empirical g -Wishart prior for sparse high-dimensional Gaussian graphical models. *arXiv preprint arXiv:1912.03807*.
- Makalic, E. and Schmidt, D. F. (2015). A simple sampler for the horseshoe estimator. *IEEE Signal Processing Letters*, 23(1):179–182.
- Meng, X.-L. and Rubin, D. B. (1993). Maximum likelihood estimation via the ECM algorithm: A general framework. *Biometrika*, 80(2):267–278.
- Park, T. and Casella, G. (2008). The Bayesian lasso. *Journal of the American Statistical Association*, 103(482):681–686.
- Piironen, J. and Vehtari, A. (2017). Sparsity information and regularization in the horseshoe and other shrinkage priors. *Electronic Journal of Statistics*, 11(2):5018–5051.
- Pourahmadi, M. (2011). Covariance estimation: The GLM and regularization perspectives. *Statistical Science*, 26(3):369–387.
- Rothman, A. J., Bickel, P. J., Levina, E., and Zhu, J. (2008). Sparse permutation invariant covariance estimation. *Electronic Journal of Statistics*, 2:494–515.
- Ryali, S., Chen, T., Supekar, K., and Menon, V. (2012). Estimation of functional connectivity in fmri data using stability selection-based sparse partial correlation with elastic net penalty. *NeuroImage*, 59(4):3852–3861.

- Song, Q. and Liang, F. (2017). Nearly optimal Bayesian shrinkage for high dimensional regression. *arXiv preprint arXiv:1712.08964*.
- Tang, X., Xu, X., Ghosh, M., and Ghosh, P. (2018). Bayesian variable selection and estimation based on global-local shrinkage priors. *Sankhya A*, 80(2):215–246.
- Tibshirani, R. (1996). Regression shrinkage and selection via the lasso. *Journal of the Royal Statistical Society. Series B*, 58:267–288.
- Wang, C., Pan, G., Tong, T., and Zhu, L. (2015). Shrinkage estimation of large dimensional precision matrix using random matrix theory. *Statistica Sinica*, 25:993–1008.
- Wang, H. (2012). Bayesian graphical lasso models and efficient posterior computation. *Bayesian Analysis*, 7(4):867–886.
- Wang, H. (2014). Coordinate descent algorithm for covariance graphical lasso. *Statistics and Computing*, 24(4):521–529.
- Weinstein, J. N., Collisson, E. A., Mills, G. B., Shaw, K. R. M., Ozenberger, B. A., Ellrott, K., Shmulevich, I., Sander, C., and Stuart, J. M. (2013). The cancer genome atlas pan-cancer analysis project. *Nature Genetics*, 45(10):1113–1120.
- Xiang, R., Khare, K., and Ghosh, M. (2015). High dimensional posterior convergence rates for decomposable graphical models. *Electronic Journal of Statistics*, 9(2):2828–2854.
- Xie, X., Kou, S. C., and Brown, L. (2016). Optimal shrinkage estimation of mean parameters in family of distributions with quadratic variance. *The Annals of Statistics*, 44(2):564–597.
- Yang, E., Ravikumar, P., Allen, G. I., and Liu, Z. (2012). Graphical models via generalized linear models. In *NIPS*, volume 25, pages 1367–1375.
- Zhang, T. and Zou, H. (2014). Sparse precision matrix estimation via lasso penalized d-trace loss. *Biometrika*, 101(1):103–120.
- Zou, H. and Hastie, T. (2005). Regularization and variable selection via the elastic net. *Journal of the Royal Statistical Society: Series B (Statistical Methodology)*, 67(2):301–320.
- Zou, H. and Li, R. (2008). One-step sparse estimates in nonconcave penalized likelihood models. *The Annals of Statistics*, 36(4):1509–1533.

Supplementary Material to

Precision Matrix Estimation under the Horseshoe-like

Prior–Penalty Dual

by

K. Sagar, S. Banerjee, J. Datta and A. Bhadra

S.1 Notations and Preliminaries

For positive real-valued sequences $\{a_n\}$ and $\{b_n\}$, $a_n = O(b_n)$ means that a_n/b_n is bounded, and $a_n = o(b_n)$ means that $a_n/b_n \rightarrow 0$ as $n \rightarrow \infty$; $a_n \lesssim b_n$ implies that $a_n = O(b_n)$, and $a_n \asymp b_n$ means that both $a_n = O(b_n)$ and $b_n = O(a_n)$ hold. For a sequence of random variables $\{X_n\}$, $X_n = O_P(\epsilon_n)$ means that $P(|X_n| \leq M\epsilon_n) \rightarrow 1$ for some constant $M > 0$.

Vectors are represented in bold lowercase English or Greek letters, with corresponding components denoted by non-bold letters, for example, $\mathbf{x} = (x_1, \dots, x_p)^T$. For a vector $\mathbf{x} \in \mathbb{R}^p$, the L_r -norm, for $0 < r < \infty$, is defined as $\|\mathbf{x}\|_r = (\sum_{i=1}^p |x_i|^r)^{1/r}$, and the L_∞ -norm is defined as $\|\mathbf{x}\|_\infty = \max_{1 \leq j \leq p} |x_j|$. The zero-vector is denoted by $\mathbf{0}$. Matrices are represented in bold uppercase English or Greek letters, for example, $\mathbf{A} = ((a_{ij}))$, where a_{ij} denotes the (i, j) th entry of \mathbf{A} . We denote the identity matrix by \mathbf{I}_p . For a symmetric matrix \mathbf{A} , $\text{eig}_1(\mathbf{A}) \leq \dots \leq \text{eig}_p(\mathbf{A})$ denote the ordered eigenvalues of \mathbf{A} , and its trace and determinant are denoted by $\text{tr}(\mathbf{A})$ and $\det \mathbf{A}$ respectively. The L_r and L_∞ -norms on $p \times p$ matrices are respectively defined as $\|\mathbf{A}\|_r = \left(\sum_{i=1}^p \sum_{j=1}^p |a_{ij}|^r \right)^{1/r}$, $0 < r < \infty$, and $\|\mathbf{A}\|_\infty = \max_{1 \leq i, j \leq p} |a_{ij}|$. In particular, the L_2 -norm, or the Frobenius norm can be expressed as $\|\mathbf{A}\|_2 = \{\text{tr}(\mathbf{A}^T \mathbf{A})\}^{1/2}$. The L_r -operator norm of \mathbf{A} is defined as $\|\mathbf{A}\|_{(r,r)} = \sup\{\|\mathbf{A}\mathbf{x}\|_r : \|\mathbf{x}\|_r = 1\}$. This gives the L_1 -operator norm as $\|\mathbf{A}\|_{(1,1)} = \max_{1 \leq j \leq p} \sum_{i=1}^p |a_{ij}|$, and the L_2 -operator norm as $\|\mathbf{A}\|_{(2,2)} = [\max_{1 \leq i \leq p} \{\text{eig}_i(\mathbf{A}^T \mathbf{A})\}]^{1/2}$, so that, for symmetric matrices, $\|\mathbf{A}\|_{(2,2)} = \max_{1 \leq i \leq p} |\text{eig}_i(\mathbf{A})|$. For a symmetric p -dimensional matrix \mathbf{A} , we have, $\|\mathbf{A}\|_\infty \leq \|\mathbf{A}\|_{(2,2)} \leq \|\mathbf{A}\|_2 \leq p\|\mathbf{A}\|_\infty$, and $\|\mathbf{A}\|_{(2,2)} \leq \|\mathbf{A}\|_{(1,1)}$. For a positive definite matrix \mathbf{A} , $\mathbf{A}^{1/2}$ denotes its unique positive square root. The diagonal matrix with the same diagonal as a matrix \mathbf{A} is denoted by \mathbf{A}^+ , and \mathbf{A}^- denotes the matrix $\mathbf{A} - \mathbf{A}^+$. The linear space of $p \times p$ symmetric matrices is denoted by \mathcal{M}_p , and $\mathcal{M}_p^+ \subset \mathcal{M}_p$ is the cone of symmetric positive definite matrices of dimension $p \times p$.

The indicator function is denoted by $\mathbb{1}$. We denote the cardinality of a finite set S by $\#S$. The

Hellinger distance between two probability densities f and g is defined as $h(f, g) = \|f^{1/2} - g^{1/2}\|_2$.

S.2 The marginal graphical horseshoe-like prior and implications for estimation algorithms

The graphical horseshoe-like prior on the individual off-diagonal elements ω_{ij} has a nice Gaussian scale mixture representation as outlined in Section 2. However, the marginal prior on these elements are not horseshoe-like, owing to the positive definite constraint on the precision matrix Ω . In this section, we argue that the hierarchical representation based on the scale-mixtures induces the proposed marginal prior on Ω and all the related marginal and conditional distributions are proper. Alongside this, we also argue that the intractable normalizing constant in the marginal prior of Ω does not affect the conditional expectation calculations for executing the expectation conditional maximization steps in our computations.

The marginal prior on Ω given the global scale parameter a can be written as,

$$\pi(\Omega \mid a) = C(a)^{-1} \prod_{i < j} \pi(\omega_{ij} \mid a) \mathbb{1}_{\mathcal{M}_p^+}(\Omega), \quad (\text{S.1})$$

where $C(a)$ is the normalizing constant depending on a . Using the Gaussian scale-mixture representation, we have a hierarchical representation of the above prior as,

$$\pi(\Omega \mid \nu, a) = C(\nu, a)^{-1} \prod_{i < j} \pi(\omega_{ij} \mid \nu_{i,j}, a) \mathbb{1}_{\mathcal{M}_p^+}(\Omega), \quad (\text{S.2})$$

where $C(\nu, a)$ is an intractable constant depending on ν and a . The prior on ν is,

$$\pi(\nu) \propto C(\nu, a) \prod_{i < j} \pi(\nu_{ij}) = C_2(a)^{-1} C(\nu, a) \prod_{i < j} \pi(\nu_{ij}), \quad (\text{S.3})$$

where $C_2(a)$ is a constant such that

$$C_2(a) = \int C(\nu, a) \prod_{i < j} \pi(\nu_{ij}) d\nu.$$

The constant $C(a)$ in (S.1) is finite because,

$$C(a) = \int \prod_{i < j} \pi(\omega_{ij} \mid a) \mathbb{1}_{\mathcal{M}_p^+}(\Omega) d(\omega_{ij})_{i \leq j} < 2K \int \prod_{i < j} \pi(\omega_{ij} \mid a) d(\omega_{ij})_{i < j} < \infty,$$

where $K < \infty$ is such that $|\omega_{ii}| < K$, ($i = 1, \dots, p$), since Ω is restricted to be positive definite and

hence the diagonal elements are finite. Also,

$$C(\nu, a) = \int \prod_{i < j} \pi(\omega_{ij} \mid \nu_{i,j}, a) \mathbb{1}_{\mathcal{M}_p^+}(\boldsymbol{\Omega}) d(\omega_{ij})_{i \leq j} < 2K \int \prod_{i < j} \pi(\omega_{ij} \mid \nu_{i,j}, a) d(\omega_{ij})_{i < j} < \infty.$$

The induced marginal prior on $\boldsymbol{\Omega}$ based on the hierarchical representation as in (S.2) and (S.3) is,

$$\pi^*(\boldsymbol{\Omega} \mid a) = C_2(a)^{-1} \prod_{i < j} \pi(\omega_{ij} \mid a) \mathbb{1}_{\mathcal{M}_p^+}(\boldsymbol{\Omega}).$$

Since $\int \pi(\boldsymbol{\Omega} \mid a) d\boldsymbol{\Omega} = \int \pi^*(\boldsymbol{\Omega} \mid a) d\boldsymbol{\Omega} = 1$, it immediately implies that $C(a) = C_2(a)$. Thus, the intractable constant $C(\nu, a)$ in (S.2) and (S.3) cancels out in the hierarchical representation, so as to arrive at the induced marginal prior (S.1). The above results also establish that the priors $\pi(\boldsymbol{\Omega} \mid a)$, $\pi(\boldsymbol{\Omega} \mid \nu, a)$, and $\pi(\nu)$ are proper.

We now show that it suffices to consider the component-wise scale-mixture representation of the horseshoe-like prior to find the conditional expectation of the latent parameters ν_{ij} in the expectation step (see equation 6) of the expectation conditional maximization algorithm. The conditional distribution of ν given $\boldsymbol{\Omega}$ and a can be written as,

$$\begin{aligned} \pi(\nu \mid \boldsymbol{\Omega}, a) &= \frac{\pi(\boldsymbol{\Omega}, \nu \mid a)}{\pi(\boldsymbol{\Omega} \mid a)} = \frac{\pi(\boldsymbol{\Omega} \mid \nu, a) \pi(\nu)}{\pi(\boldsymbol{\Omega} \mid a)} \\ &= \frac{\prod_{i < j} \pi(\omega_{ij} \mid \nu_{ij}, a) \prod_{i < j} \pi(\nu_{ij}) \mathbb{1}_{\mathcal{M}_p^+}(\boldsymbol{\Omega})}{\prod_{i < j} \pi(\omega_{ij} \mid a) \mathbb{1}_{\mathcal{M}_p^+}(\boldsymbol{\Omega})}. \end{aligned}$$

This gives,

$$\pi(\nu_{ij} \mid \boldsymbol{\Omega}, a) = \frac{\pi(\omega_{ij} \mid \nu_{ij}, a) \pi(\nu_{ij})}{\pi(\omega_{ij} \mid a)} \mathbb{1}_{\mathcal{M}_p^+}(\boldsymbol{\Omega}).$$

Thus, the expectation step (6) holds given that the conditional maximization step produces positive definite estimates of $\boldsymbol{\Omega}$ in each iteration.

S.3 Auxiliary Lemmas

Lemma S.3.1. *Let p_k denote the density of a $\mathcal{N}_d(\mathbf{0}, \boldsymbol{\Sigma}_k)$ random variable, $k = 1, 2$. Denote the corresponding precision matrices by $\boldsymbol{\Omega}_k = \boldsymbol{\Sigma}_k^{-1}$, $k = 1, 2$. Then,*

$$\begin{aligned} \mathbb{E}_{p_1} \left\{ \log \frac{p_1}{p_2}(\mathbf{X}) \right\} &= \frac{1}{2} \{ \log \det \boldsymbol{\Omega}_1 - \log \det \boldsymbol{\Omega}_2 + \text{tr}(\boldsymbol{\Omega}_1^{-1} \boldsymbol{\Omega}_2) - d \}, \\ \text{Var}_{p_1} \left\{ \log \frac{p_1}{p_2}(\mathbf{X}) \right\} &= \frac{1}{2} \text{tr} \{ (\boldsymbol{\Omega}_1^{-1/2} \boldsymbol{\Omega}_2 \boldsymbol{\Omega}_1^{-1/2} - \mathbf{I}_d)^2 \}. \end{aligned}$$

Proof. Let us define $\mathbf{A} = \mathbf{\Omega}_1^{-1/2} \mathbf{\Omega}_2 \mathbf{\Omega}_1^{-1/2}$. Note that, for a random variable $\mathbf{Z} \sim \mathcal{N}_d(\mathbf{0}, \mathbf{\Sigma})$, we have,

$$\mathbb{E}(\mathbf{Z}^T \mathbf{A} \mathbf{Z}) = \text{tr}(\mathbf{A} \mathbf{\Sigma}), \quad \text{Var}(\mathbf{Z}^T \mathbf{A} \mathbf{Z}) = 2 \text{tr}(\mathbf{A} \mathbf{\Sigma} \mathbf{A} \mathbf{\Sigma}).$$

Then, for $\mathbf{X} \sim \mathcal{N}_d(\mathbf{0}, \mathbf{\Sigma}_1)$,

$$\begin{aligned} \mathbb{E}_{p_1} \left\{ \log \frac{p_1}{p_2}(\mathbf{X}) \right\} &= \frac{1}{2} \{ \log \det \mathbf{\Omega}_1 - \log \det \mathbf{\Omega}_2 + \mathbb{E}_{p_1}(\mathbf{X}^T (\mathbf{\Omega}_2 - \mathbf{\Omega}_1) \mathbf{X}) \} \\ &= \frac{1}{2} \{ \log \det \mathbf{\Omega}_1 - \log \det \mathbf{\Omega}_2 + \text{tr}[(\mathbf{\Omega}_2 - \mathbf{\Omega}_1) \mathbf{\Sigma}_1] \} \\ &= \frac{1}{2} \{ \log \det \mathbf{\Omega}_1 - \log \det \mathbf{\Omega}_2 + \text{tr}(\mathbf{\Omega}_1^{-1} \mathbf{\Omega}_2) - d \}. \end{aligned}$$

Also,

$$\begin{aligned} \text{Var}_{p_1} \left\{ \log \frac{p_1}{p_2}(\mathbf{X}) \right\} &= \mathbb{E}_{p_1} \left[\log \frac{p_1}{p_2}(\mathbf{X}) - \mathbb{E}_{p_1} \left\{ \log \frac{p_1}{p_2}(\mathbf{X}) \right\} \right]^2 \\ &= \frac{1}{4} \mathbb{E}_{p_1} \{ \mathbf{X}^T (\mathbf{\Omega}_2 - \mathbf{\Omega}_1) \mathbf{X} - \mathbb{E}_{p_1}(\mathbf{X}^T (\mathbf{\Omega}_2 - \mathbf{\Omega}_1) \mathbf{X}) \}^2 \\ &= \frac{1}{4} \text{Var}_{p_1} \{ \mathbf{X}^T (\mathbf{\Omega}_2 - \mathbf{\Omega}_1) \mathbf{X} \} \\ &= \frac{1}{4} 2 \text{tr} \{ (\mathbf{\Omega}_2 - \mathbf{\Omega}_1) \mathbf{\Omega}_1^{-1} (\mathbf{\Omega}_2 - \mathbf{\Omega}_1) \mathbf{\Omega}_1^{-1} \} \\ &= \frac{1}{2} \text{tr} \{ (\mathbf{\Omega}_1^{-1/2} \mathbf{\Omega}_2 \mathbf{\Omega}_1^{-1/2} - \mathbf{I}_d)^2 \}. \end{aligned}$$

□

Lemma S.3.2. Consider the horseshoe-like prior $\pi(\theta \mid a)$. Then, for the global shrinkage parameter a satisfying the condition $a < p^{-2b_1}/n$ for some constant $b_1 > 0, \nu > 0$, we have,

$$1 - \int_{-\epsilon_n/p^\nu}^{\epsilon_n/p^\nu} \pi(\theta \mid a) d\theta \leq p^{-b'_1}, \quad (\text{S.4})$$

for some constants $\nu, b'_1 > 0$. Additionally, for some sufficiently large constant $B \sim b_2 n \epsilon_n^2$, if the global scale parameter satisfies the condition $a/B^2 < p^{-2b_3}$ for some constant $b_3 > 0$, we have,

$$-\log \left(\int_{|\theta| > B} \pi(\theta \mid a) d\theta \right) \gtrsim B. \quad (\text{S.5})$$

Proof. We have,

$$1 - \int_{-\epsilon_n/p^\nu}^{\epsilon_n/p^\nu} \pi(\theta \mid a) d\theta = \int_{|\theta| > \epsilon_n/p^\nu} \pi(\theta \mid a) d\theta$$

$$\begin{aligned}
&= \int_{|\theta| > \epsilon_n/p^\nu} \frac{1}{2\pi a^{1/2}} \log \left(1 + \frac{a}{\theta^2} \right) d\theta \\
&= 2 \int_{\epsilon_n/p^\nu}^{\infty} \frac{1}{2\pi a^{1/2}} \log \left(1 + \frac{a}{\theta^2} \right) d\theta \\
&\leq \int_{\epsilon_n/p^\nu}^{\infty} \frac{1}{\pi a^{1/2}} \frac{a}{\theta^2} d\theta = \frac{2}{\pi} \frac{a^{1/2} p^\nu}{\epsilon_n}.
\end{aligned}$$

Note that, for $a^{1/2} < n^{-1/2} p^{-b_1}$, the right hand side of the display above is bounded by $p^{-b'_1}$, for $0 < b'_1 \leq b_1 - \nu$. This proves the first part of the lemma. For the second part, note that,

$$\int_{|\theta| > B} \pi(\theta | a) d\theta \leq \frac{2}{\pi} \frac{a^{1/2}}{B}.$$

Hence, for the condition $a^{1/2}/B < p^{-b_3}$, we have,

$$\int_{|\theta| > B} \pi(\theta | a) d\theta \lesssim p^{-b_3} = \exp(-b_3 \log p) \lesssim \exp(-b_2 n \epsilon_n^2),$$

which implies that, for $B \sim b_2 n \epsilon_n^2$,

$$-\log \left(\int_{|\theta| > B} \pi(\theta | a) d\theta \right) \gtrsim B.$$

This completes the proof. \square

Corollary S.3.3. *The above lemma holds true under the same conditions on the global shrinkage parameter for the horseshoe prior as well.*

Proof. Note that the prior density of the horseshoe prior satisfies

$$p_{HS}(\theta | a) < \frac{2}{a^{1/2} (2\pi)^{3/2}} \log \left(1 + \frac{2a}{\theta^2} \right), \quad (\text{S.6})$$

which implies that, retracing the steps in the proof of Lemma S.3.2 above,

$$\int_{|\theta| > t} p_{HS}(\theta | a) d\theta \lesssim \frac{a^{1/2}}{t}. \quad (\text{S.7})$$

The result thus follows immediately. \square

We now present the Gershgorin Circle Theorem ([Brualdi and Mellendorf, 1994](#)), that will be required in the proof of our main result on posterior convergence rate. The actual theorem holds for complex matrices, but we only need the result for real matrices.

Theorem S.3.4 (Gershgorin Circle Theorem for real matrices). *Let $\mathbf{A} = ((a_{ij}))$ be a p -dimensional real-valued matrix with real eigenvalues. Define $R_i = \sum_{j \neq i} |a_{ij}|$, $i = 1, \dots, p$, the row sums of the absolute entries of \mathbf{A} excluding the diagonal element. Then, each eigenvalue of \mathbf{A} is in at least one of the disks*

$$\mathcal{D}_i(\mathbf{A}) = \{z: |z - a_{ii}| \leq R_i\}, \quad 1 \leq i \leq p.$$

Equivalently, the p eigenvalues of \mathbf{A} are contained in the region in the real plane determined by

$$\mathcal{D}(\mathbf{A}) = \cup_{i=1}^p \mathcal{D}_i(\mathbf{A}).$$

Proof. The eigenvalue equation for \mathbf{A} is given by $\mathbf{A}\mathbf{x} = \lambda\mathbf{x}$, where λ is an eigenvalue of \mathbf{A} and $\mathbf{x} = (x_1, \dots, x_p)^T \in \mathbb{R}^p$ is the corresponding non-zero eigenvector. Let us consider $1 \leq m \leq p$ such that $|x_m| = \|\mathbf{x}\|_\infty$. Then, the above eigenvalue equation implies that, $\sum_{j=1}^p a_{mj}x_j = \lambda x_m$. Rearranging the terms, we get, $\sum_{j \neq m} a_{mj}x_j = (\lambda - a_{mm})x_m$, which implies that,

$$|\lambda - a_{mm}||x_m| = \left| \sum_{j \neq m} a_{mj}x_j \right| \leq \sum_{j \neq m} |a_{mj}||x_j| \leq |x_m| \sum_{j \neq m} |a_{mj}|.$$

Hence, for any eigenvalue λ of \mathbf{A} , we have, $|\lambda - a_{mm}| \leq \sum_{j \neq m} |a_{mj}|$. Thus, each of the p eigenvalues of \mathbf{A} must lie in at least one of the disks $\mathcal{D}_i(\mathbf{A})$ as defined in the theorem above. This completes the proof. \square

Lemma S.3.5. *For the graphical horseshoe-like prior (2), under the assumption that the global scale parameter satisfies the condition $a^{1/2} < L^{-1}n^{-1/2}p^{-(2+u)}$, $u > 0$, the prior probability owing to the constraint $\boldsymbol{\Omega} \in \mathcal{M}_p^+(L)$ has the lower bound*

$$\Pi(\boldsymbol{\Omega} \in \mathcal{M}_p^+(L)) \gtrsim L^p \exp\left(-C_1 n^{-1/2} p\right), \quad (\text{S.8})$$

for some suitable constant $C_1 > 0$.

Proof. We shall use the Gershgorin Circle theorem presented in Theorem S.3.4. Each of the eigenvalues of $\boldsymbol{\Omega}$, given by $\text{eig}_1(\boldsymbol{\Omega}) \leq \dots \leq \text{eig}_p(\boldsymbol{\Omega})$, lies in the interval $\cup_{j=1}^p \left[\omega_{jj} \mp \sum_{k=1, k \neq j}^p |\omega_{kj}| \right]$. This implies,

$$\Pi(\boldsymbol{\Omega} \in \mathcal{M}_p^+(L)) \geq \Pi\left(\min_j (\omega_{jj} - \sum_{k=1, k \neq j}^p |\omega_{kj}|) > 0, \boldsymbol{\Omega} \in \mathcal{M}_p^+(L)\right).$$

For the constraint that $\min_j(\omega_{jj} - \sum_{k=1, k \neq j}^p |\omega_{kj}|) > 0$,

$$\text{eig}_p(\mathbf{\Omega}) = \|\mathbf{\Omega}\|_{(2,2)} \leq \|\mathbf{\Omega}\|_{(1,1)} = \max_j(\omega_{jj} + \sum_{k=1, k \neq j}^p |\omega_{kj}|) \leq 2 \max_j \omega_{jj},$$

and,

$$\text{eig}_1(\mathbf{\Omega}) \geq \min_j(\omega_{jj} - \sum_{k=1, k \neq j}^p |\omega_{kj}|).$$

Thus,

$$\begin{aligned} & \Pi(\mathbf{\Omega} \in \mathcal{M}_p^+(L)) \\ & \geq \Pi(L^{-1} \leq \min_j(\omega_{jj} - \sum_{k=1, k \neq j}^p |\omega_{kj}|) \leq 2 \max_j \omega_{jj} \leq L) \\ & \geq \Pi(L^{-1} \leq \min_j(\omega_{jj} - L^{-1}) \leq 2 \max_j \omega_{jj} \leq L \mid \max_{k \neq j} |\omega_{kj}| < (Lp)^{-1}) \Pi(\max_{k \neq j} |\omega_{kj}| < (Lp)^{-1}) \\ & = \Pi(L^{-1} \leq \min_j(\omega_{jj} - L^{-1}) \leq 2 \max_j \omega_{jj} \leq L) \Pi(\max_{k \neq j} |\omega_{kj}| < (Lp)^{-1}). \end{aligned} \quad (\text{S.9})$$

Note that,

$$\begin{aligned} \Pi(L^{-1} \leq \min_j(\omega_{jj} - L^{-1}) \leq 2 \max_j \omega_{jj} \leq L) & \geq \Pi(2L^{-1} \leq \omega_{jj} \leq L/2, 1 \leq j \leq p) \\ & = \prod_{j=1}^p \Pi(2L^{-1} \leq \omega_{jj} \leq L/2) \sim L^p. \end{aligned} \quad (\text{S.10})$$

Also, from (S.4) in Lemma S.3.2, we get,

$$\begin{aligned} \Pi(\max_{k \neq j} |\omega_{kj}| < (Lp)^{-1}) & = \prod_{k \neq j} \{1 - \Pi(|\omega_{kj}| > (Lp)^{-1})\} \\ & \geq (1 - C_0 a^{1/2} Lp)^{p^2} \geq \exp(-C_1 a^{1/2} Lp^3) \\ & \geq \exp(-C_1 n^{-1/2} p). \end{aligned} \quad (\text{S.11})$$

The last inequality follows from the fact that $a^{1/2} < L^{-1} n^{-1/2} p^{-(2+u)}$, $u > 0$. Therefore, combining (S.9), (S.10) and (S.11), we get, $\Pi(\mathbf{\Omega} \in \mathcal{M}_p^+(L)) \gtrsim L^p \exp(-C_1 n^{-1/2} p)$, thus completing the proof. \square

Corollary S.3.6. *The above lemma holds true for the graphical horseshoe prior as well under the same conditions on the global shrinkage parameter.*

Proof. The proof of this result is exactly similar to that of Lemma S.3.5. The lower bound on the off-diagonal entries follows immediately from Corollary S.3.3. The rest of the arguments remain

intact. □

Lemma S.3.7 (Lemma A.3 in [Bickel and Levina \(2008\)](#)). Let $\mathbf{Z}_i \stackrel{iid}{\sim} \mathcal{N}_p(\mathbf{0}, \mathbf{\Sigma})$, $\text{eig}_p(\mathbf{\Sigma}) \leq \varepsilon_0 < \infty$. Then, if $\mathbf{\Sigma} = ((\sigma_{ij}))$,

$$\Pr \left[\left| \sum_{i=1}^n Z_{ij} Z_{ik} - \sigma_{jk} \right| \geq nt \right] \leq c_1 \exp(-c_2 nt^2), \quad |t| \leq \delta,$$

where c_1, c_2 and δ depend on ε_0 only.

S.4 Proof of Corollary 4.7

The proof of this result is exactly similar to that of Theorem 4.6. The proof of the latter relies on Lemma S.3.2 and Lemma S.3.5 that are specific to the graphical horseshoe-like prior, and the corollaries given by Corollary S.3.3 and Corollary S.3.6 are respectively their counterparts corresponding to the graphical horseshoe prior. The utilization of the general lemma on Kullback–Leibler distance computations as outlined in Lemma S.3.1 remains identical in the present case.

S.5 Proof of Lemma 4.8

We will prove concavity by proving the second derivative is negative. By direct calculations:

$$\frac{d^2}{dx^2}(\text{pen}_a(x)) = \frac{d^2}{dx^2}(-\log \log(1 + \frac{a}{x^2})) = -\frac{2a((a + 3x^2)\log(1 + a/x^2) - 2a)}{x^2(a + x^2)^2(\log^2(1 + a/x^2))}. \quad (\text{S.12})$$

Since the denominator of the RHS in (S.12) is always positive, we can investigate the sign of the double derivative of the above penalty function by considering only the numerator, and furthermore as $a > 0$, we need the following to hold to prove concavity:

$$(a + 3x^2)\log(1 + a/x^2) - 2a \geq 0. \quad (\text{S.13})$$

Substituting $\log(1 + a/x^2)$ by z , so that $x^2 = a/(\exp(z) - 1)$, we have $z \geq 0$, and the RHS of (S.13) is given by,

$$\begin{aligned} (a + 3x^2)\log(1 + a/x^2) - 2a &= \left(a + \frac{3a}{\exp(z) - 1}\right)z - 2a \\ &= a \left(\frac{3z + (z - 2)(\exp(z) - 1)}{\exp(z) - 1}\right) \\ &> a \left(\frac{z(1 + z)}{\exp(z) - 1}\right) > 0, \quad \text{since } \exp(z) > 1 + z. \end{aligned}$$

This proves the (strict) concavity of the graphical horseshoe-like penalty function.

S.6 Estimating the Global Scale Parameter

We use the technique of [Piironen and Vehtari \(2017\)](#) to tune the global parameter for GHS-LIKE-ECM via an estimate of the *effective model size*. Consider a linear regression model $y_i = \boldsymbol{\theta}^T \mathbf{x}_i + \epsilon_i$, $\epsilon_i \sim \mathcal{N}(0, \sigma^2)$ for $i = 1, \dots, n$, where $\boldsymbol{\theta} = \{\theta_j\}$ and \mathbf{x}_i are p -dimensional vectors. Consider the global-local shrinkage priors of the form $\theta_j \sim \mathcal{N}(0, \lambda_j^2 a)$, $\lambda_j \sim \pi(\lambda_j)$. Then, assuming the design matrix to be orthogonal, the shrinkage estimates of the elements of $\boldsymbol{\theta}$ can be written as, $\bar{\theta}_j = (1 - \kappa_j) \hat{\theta}_j$. In this context, κ_j is called shrinkage coefficient, which takes the form $(1 + n\sigma^{-2}\tau^2\lambda_j^2)^{-1}$ and $\hat{\theta}_j$ is the ordinary least squares (OLS) estimate. For the horseshoe-like prior, $\pi(\theta_j | u_j, a) \sim \mathcal{N}(0, a/(2u_j))$, and $\pi(u_j) = (1 - \exp(-u_j))/(2\pi^{1/2}u_j^{3/2})$. Hence, the shrinkage coefficient is $(1 + n\sigma^{-2}a(2u_j)^{-1})^{-1}$.

[Piironen and Vehtari \(2017\)](#) define the effective model size as $m_{\text{eff}} = \sum_{j=1}^p (1 - \kappa_j)$. In order to compute the global scale parameter a or to decide a prior for it, they set $\mathbb{E}(m_{\text{eff}}) = p_0$, which is the expected number of non-zero elements in $\boldsymbol{\theta}$. In the context of our problem, we need to find an expression for $\mathbb{E}(\kappa_j)$ in order to solve for a in $\mathbb{E}(m_{\text{eff}}) = p_0$. Using the standard Jacobian technique we get the density of κ_j as,

$$\pi(\kappa_j) = \frac{1}{2\pi^{1/2}} \kappa_j^{-3/2} (1 - \kappa_j)^{-1/2} \left(\frac{na}{2\sigma^2} \right)^{-1/2} \left\{ 1 - \exp \left(-\frac{\kappa_j}{1 - \kappa_j} \frac{na}{2\sigma^2} \right) \right\}.$$

After some trivial variable transforms, $\mathbb{E}(\kappa_j | a)$ can be written as,

$$\mathbb{E}(\kappa_j | a) = \frac{2\sigma}{(2\pi na)^{1/2}} \int_0^{\pi/2} \left\{ 1 - \exp \left(-\frac{na}{2\sigma^2} \tan^2 \eta \right) \right\} d\eta.$$

As a closed form solution of the above integral is not available, we set $na(2\sigma^2)^{-1} = m^2$ and approximate $\exp(-na \tan^2 \eta / (2\sigma^2))$ by a polynomial of order 16 using Taylor's series about $\eta = 0$. After integrating the approximated polynomial with respect to η , we get a polynomial of order 31 in m to solve for the value of global scale parameter a . Thus, $\mathbb{E}(m_{\text{eff}}) = p_0$ gives,

$$1 - \sum_{r=0}^{31} c_r m^r = \frac{p_0}{p},$$

where c_r , $r = 0, \dots, 31$ are the coefficients of the polynomial which are obtained after Taylor's expansion followed by integration. In all our simulations and real data applications, we fix $p_0/p = 2/(p-1)$ and assume that $\sigma^2 = 1$. For a given value of (n, p) , we can get a value for the global

scale parameter $a = 2m^2/n$ by solving the above equation for m . For our simulations and real data application, we got 15 pairs of complex conjugates while solving the above equation (in \mathbb{R} , using function `polyroot()`) and only one real positive value for m . The values of global scale parameter hence obtained for simulations and real data experiment are as follows:

1. **Table 1, 2:** $(n, p) = (120, 100)$, estimate of the global scale parameter $a = 0.0143$.
2. **Table 3, 4:** $(n, p) = (120, 200)$, estimate of the global scale parameter $a = 0.0169$.
3. **Proteomics Data:** $(n, p) = (33, 67)$, estimate of the global scale parameter $a = 0.0519$.

S.7 Diagnostics: Choice of Starting Values for the ECM Algorithm and Trace Plots for the ECM and MCMC Algorithms

Since the likelihood surface under the GHS-Like prior is likely highly multi-modal, and the ECM algorithm is only guaranteed to find a local mode, we provide additional numerical results investigating the effect of starting values on the estimates. Given a true precision matrix Ω_0 and $(n, p) = (50, 100)$ we generate 50 data sets, and perform estimation with 1, 10, 20 and 50 randomly chosen starting points. The accuracy measures of these estimates are represented as 1*, 10*, 20* and 50* in the Table S.1. In general, we observe that the estimates from 50 different starting points perform the best in terms of Stein’s loss, Frobenius norm, and TPR; while being slightly worse in terms of FPR and MCC.

In the presence of a highly multimodal likelihood surface, it is safe to believe that true signal which might be missed for any given starting point. Hence averaging across different starting values leads to an improvement in terms of most metrics and this what we choose to follow in our examples. Nevertheless, it is reassuring to see the final results are not too sensitive to the choice of starting values.

Further, Figure S.1 shows a sample trace plot of log-likelihood when the precision matrix was estimated for a representative data set using GHS-LIKE-ECM and GHS-LIKE-MCMC. It is apparent that convergence to a local maximum (for ECM) and to the stationary distribution (for MCMC) occur relatively quickly. Similar behavior was observed in all other settings.

S.8 Additional Details on the Proteomics Data

Table S.2 provides the map between the node numbers and protein names in Figure 2.

Table S.1: Mean (sd) Stein’s loss, Frobenius norm, true positive rates and false positive rates, Matthews Correlation Coefficient of precision matrix estimates for GHS-LIKE-ECM over 50 data sets with $p = 100$ and $n = 50$. The best performer in each row is shown in bold. Average CPU time is in seconds.

nonzero pairs nonzero elements $p = 100, n = 50$	Random 35/4950 $\sim -\text{Unif}(0.2, 1)$				Hubs 90/4950 0.25			
	1*	10*	20*	50*	1*	10*	20*	50*
Stein’s loss	9.624 (0.915)	8.503 (0.801)	8.196 (0.749)	8.302 (0.749)	12.563 (0.83)	10.494 (0.885)	10.408 (0.831)	10.268 (0.81)
F norm	3.674 (0.237)	3.344 (0.191)	3.286 (0.191)	3.279 (0.178)	4.166 (0.197)	3.672 (0.188)	3.645 (0.171)	3.616 (0.174)
TPR	0.703 (0.044)	0.816 (0.042)	0.814 (0.046)	0.825 (0.039)	0.551 (0.049)	0.756 (0.053)	0.766 (0.054)	0.772 (0.053)
FPR	0.021 (0.002)	0.054 (0.004)	0.058 (0.004)	0.063 (0.005)	0.015 (0.002)	0.038 (0.004)	0.041 (0.004)	0.044 (0.004)
MCC	0.329 (0.024)	0.271 (0.014)	0.26 (0.013)	0.253 (0.011)	0.464 (0.034)	0.435 (0.027)	0.426 (0.025)	0.419 (0.023)
Avg CPU time	6.735	5.378
nonzero pairs nonzero elements $p = 100, n = 50$	Cliques negative 30/4950 -0.45				Cliques positive 30/4950 0.75			
	1*	10*	20*	50*	1*	10*	20*	50*
Stein’s loss	9.149 (0.774)	7.417 (0.673)	7.276 (0.673)	7.289 (0.67)	13.896 (1.032)	9.156 (0.83)	8.719 (0.822)	8.65 (0.848)
F norm	3.746 (0.265)	3.231 (0.263)	3.18 (0.215)	3.174 (0.255)	5.453 (0.245)	4.178 (0.241)	3.995 (0.268)	3.974 (0.261)
TPR	0.911 (0.029)	0.995 (0.012)	0.999 (0.005)	1 (0)	0.741 (0.048)	0.997 (0.001)	0.997 (0.01)	0.997 (0.01)
FPR	0.021 (0.002)	0.053 (0.004)	0.058 (0.005)	0.064 (0.005)	0.023 (0.002)	0.051 (0.003)	0.055 (0.004)	0.059 (0.005)
MCC	0.433 (0.016)	0.312 (0.013)	0.3 (0.012)	0.287 (0.011)	0.344 (0.024)	0.318 (0.009)	0.308 (0.01)	0.298 (0.01)
Avg CPU time	5.08	5.088

Table S.2: Map between node numbers and protein names in Figure 2.

1 BAK1	11 MYH11	21 PCNA	31 TP53	41 ATK1S1	51 MAPK14	61 MTOR
2 BAX	12 RAB11A, RAB11B	22 FOXM1	32 RAD50	42 TSC2	52 RPS6KA1	62 RPS6
3 BID	13 CTNNB1	23 CDH1	33 RAD51	43 INPP4B	53 YBX1	63 RB1
4 BCL2L11	14 GADPH	24 CLDN7	34 XRCC1	44 PTEN	54 EGFR	64 ESR1
5 CASP7	15 RBM15	25 TP53BP1	35 FN1	45 ARAF	55 ERBB2	65 PGR
6 BAD	16 CDK1	26 ATM	36 CDH2	46 JUN	56 ERBB3	66 AR
7 BCL2	17 CCNB1	27 CHEK1	37 COL6A1	47 RAF1	57 SHC1	67 GATA3
8 BCL2L1	18 CCNE1	28 CHEK2	38 SERPINE1	48 MAPK8	58 SRC	
9 BIRC2	19 CCNE2	29 XRCC5	39 ATK1, ATK2, ATK3	49 MAPK1, MAPK3	59 EIF4EBP1	
10 CAV1	20 CDKN1B	30 MRE11A	40 GKS3A, GKS3B	50 MAP2K1	60 RPS6KB1	

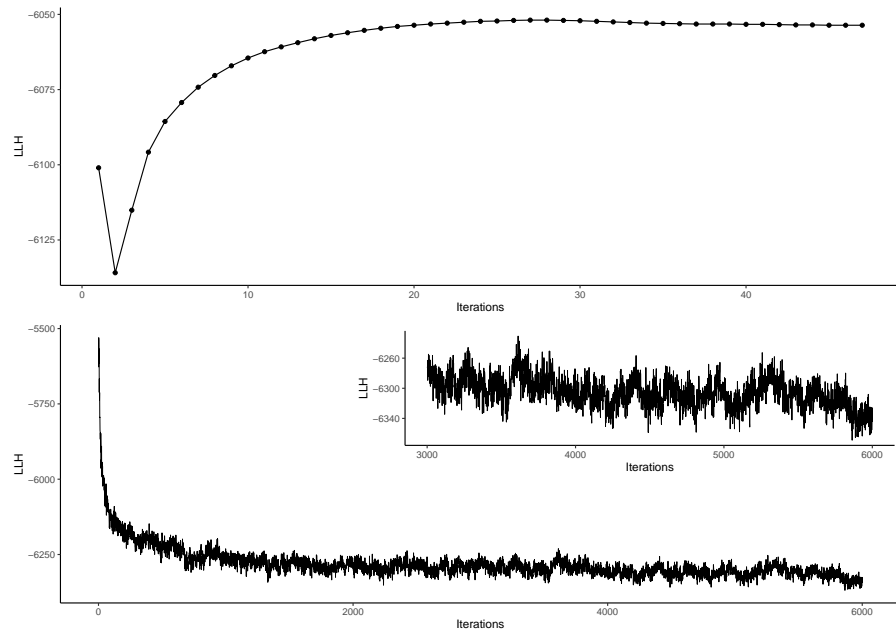


Figure S.1: Top and bottom panels show the plot of log-likelihood (LLH) vs. Iterations when the precision matrix was estimated for a representative data set using GHS-LIKE-ECM and GHS-LIKE-MCMC procedures respectively, for 'Hubs' structure when $n = 120$, $p = 100$. The inset plot in the bottom panel shows the zoomed-in version of the plot after the burn-in period.